Effect of Solutes on Grain Refinement

Z. Fan, F. Gao, Y. Wang, H. Men, L. Zhou

BCAST, Brunel University London, Uxbridge, Middlesex, UB8 3PH, UK.

Abstract:

Grain refinement not only enhances the mechanical performance of as-cast metallic materials but also provides an effective mechanism for controlling cast defects, such as macro-segregation, porosity and coarse second phase particles. Therefore, understanding grain refinement of alloys with different solute additions is of both theoretical and practical importance. Although extensive research has been carried out over many decades and significant progress has been made on the subject, such historical research has not delivered the desirable scientific understanding, and many critical questions remain open. Adopting a hybrid approach between review and overview, in this paper, we firstly provide a brief review on the historical research on the solute effect on grain refinement in the literature, then present the recent advances in the understanding of the subject in a holistic manner, and finally offer a summary of the factors that hindered progress in the past, key advances made in recent years and some suggestions for future research directions.

Keywords: Composition; Grain refinement; Nucleation; Grain initiation; Growth restriction.

1. Introduction

All metallic materials start their life with solidification processing, where the metallic materials are either cast into components for direct engineering applications or feedstock materials for further thermomechanical processing. In both cases, it is usually desirable to have a fine and uniform grain structure in the as-cast state since such a grain refined microstructure provides not only enhanced mechanical properties but also an effective mechanism for controlling the cast defects, such as macro-segregation, porosity and coarse second phase particles [1,2]. Therefore, understanding grain refinement is of both theoretical and practical importance.

Grain refinement is defined as deliberate suppression of columnar grain growth in ingots and castings and formation of fine equiaxed grain structure throughout the material [1]. Grain refinement is usually achieved by addition of grain refiners that contain potent nucleant particles prior to the casting process. As demonstrated in Fig. 1, commercial purity Al (CP-Al, containing 0.15-0.3wt.% impurity elements, mainly Fe and Si) has a coarse columnar grain structure, being a typical non-refined grain structure (Fig. 1a), while CP-Al with 0.2wt.% addition of Al-5Ti-1B grain refiner exhibits a typical refined grain structure containing fine equiaxed grains (Fig. 1b) [3]. However, the addition of 580 ppm Zr to CP-Al reverses a grain-refined structure (Fig. 1b) to a non-refined grain structure (Fig. 1c), rendering Al-5Ti-1B grain refiner being no longer effective for grain refinement [4], which is referred to as Zr-poisoning in the literature [5-9]. Similarly, addition of more than 3wt.% Si to CP-Al leads to a coarse equiaxed grain structure (Fig. 1d) [10], and this is the so-called Si-poisoning [8, 11-14]. Up to now, the mechanisms for both grain refinement and poisoning by Zr or Si have been widely investigated and it is generally recognised that two factors play a critical role in delivering grain refinement: the

presence of solute in the melt, and the existence of solid particles which can act as the substrates for heterogeneous nucleation during solidification processing [15-20].

So far, a great deal of experimental work has been carried out to understand the relationship between the solute contents and grain size in Al-alloys [21-29], Mg-alloys [30-32], Zn-alloys [33-36], Ti-alloys [37-39] and Cu-alloys [40-43]. In order to quantify the solute effect, a number of empirical or semi-empirical parameters, such as P (constitutional supercooling parameter), Q (growth restriction factor) and ΔT (freezing range), have been proposed and applied to describe the relationship between as-cast grain size and the solute contents. Meanwhile, theoretical models have also been developed to elucidate the solute effect on grain refinement [44-53]. Although certain agreement exists between model predictions and experimental data, there are still many open questions about grain refinement in both scientific understanding and industrial practice. For example, Tarshis *et al.* [21] proposed a parameter, P, to quantify the solute effect and correlate grain size with P in Ni- and Al-based alloys. This parameter was also used by Spittle and Sadli [23], who suggested that there appeared to be a good correlation between grain size and P. However, a number of studies [47-50] suggested that grain size was inversely proportional to the growth restriction factor Q. Becerra and Pekguleryuz [31] found experimentally that grain size was related to Q in Mg-Zn alloys, but in Mg-In alloys, the grain size was better described as a function of $(1/Q)^{1/3}$. Xu *et al.* [27] compared experimentally the relationships between grain size and three parameters (i.e. P, Q and ΔT) of Al-alloys, and pointed out that the measured grain size was more closely related to ΔT rather than P and Q. In addition, it is also reported that all these relationships shown above obtained from Al- and Mg-alloys are not applicable to Zn alloys [33].

Besides the inconsistency in experimental results, discrepancies also arise in theoretical models. Some models [47-50] suggest that grain size is inversely proportioned to Q. However, Men and Fan [51] revealed that grain size could be simply related to $(1/Q)^{1/3}$ under isothermal solidification. Shu *et al.* [52] developed a numerical model to predict the grain size of cast Al alloys, suggesting that the grain refinement of alloys of high solute content was controlled primarily by solute suppressed nucleation zone (SSNZ). However, Du and Li [53] argued that in their numerical model based on the Kampmann-Wagner model [54] the SSNZ effect could be neglected during isothermal solidification, where nucleation is stifled by recalescence.

Spittle and Sadli [23] conducted the first systematic investigation of the effect of solute contents on grain refinement of Al-alloys using the Alcan TP-1 tests [55], and they found that solute addition could lead to significant grain refinement. For instance, the grain size was reduced from 1200μm for high purity Al (HP-Al) to about 110μm with addition of solute elements. However, in their work [23] grain size data were obtained from the cross-section of the as-cast samples without checking the microstructure in the vertical sections. As pointed out in Refs. [3, 56], an equiaxed grain structure in the cross-section is insufficient to ensure an equiaxed grain structure in the entire as-cast sample (e.g. Fig. 1a).

Grain refinement is a complex phenomenon [57], depending on not only solutes in the melt but also the physical and chemical nature of the nucleant particles that may be either endogenous or exogenous [57]. This means that studies on the solute effect on grain refinement without consideration of nucleant particles will be insufficient to ensure sound conclusions. In addition, under usual solidification condition relevant to industrial practice, the grain structure is largely determined by early stages of solidification, which occurs within a fraction of a second, a solid fraction less than 10^{-4} and solid particle size smaller than a few microns. Generally, as suggested by Fan *et al.* [58], the early stage of solidification mainly includes the prenucleation, nucleation, grain initiation, spherical growth and recalescence, as schematically illustrated in Fig. 2 [58]. Therefore, the effect of solute at any of such stages may affect the final grain structure of the solidified alloy.

In this paper, we firstly provide a brief review of the historical research on the solute effect on grain refinement in the literature, then present advances in the understanding of the subject in a holistic manner, and finally offer some suggestions for future research directions. This means that we offer a hybrid between review and overview. This makes it impossible to provide a full coverage of the literature on the subject, for which the readers are directed to the recent review papers, such as Refs. [15-20].

2. Historical research

2.1 Grain refining mechanism of Al-Ti-B master alloy for Al-alloys

Al-Ti-B master alloy is the most widely used grain refiner for Al-alloys, and effects of both nucleant particles (TiB_2) and solute Ti on grain refinement have been extensively researched. In his seminal research work, Cibula [59,60] studied the mechanism of grain refinement of Al-alloys with addition of Ti, and pointed out that the presence of Ti, particularly in combination with carbon or boron, produced a good grain refining effect in Al, where the carbides and borides provided the heterogeneous nucleation sites due to the close match of atomic spacings on the close-packed planes between the substrates and Al marking the beginning of the Al-Ti-B as a grain refiner system. However, this conclusion about nucleant particles was challenged by the subsequent researchers. Crossley and Mondol [61], Mascre *et al.* [62] and Nakao [63] found that the heavy addition of carbon to Al-Ti alloys reduced the grain refining effect, which was inconsistent with the findings of Cibula [59]. Seeman and Staats [64] reported that there was no grain refinement with additions of TiB_2 or VC, but refinement with Ti, TiC, or Ti+TiB_2. Moriceau [65] concluded that TiB_2 could nucleate Al based on the microprobe photographs. However, Marcantonio and Mondolfo [66] considered that in Moriceau's work [65] the particles in the boron-rich zone was considerably smaller than that in the Ti-rich zone, indicating that Al is diffusing into the TiB_2 and Ti out of it so that the actual particles consist of a core of (Al, Ti)B_2 sheathed by Al_3Ti which can nucleate Al crystal [67] as there is epitaxy between them.

However, during the grain refinement of Al-alloys using Al-Ti-B master alloys, the amount of free Ti added to the melt via the master alloy is usually less than 0.01wt.%, which is much lower than the Ti level required for peritectic reaction (0.15wt.%), suggesting that Al_3Ti is not thermodynamically stable. Davies [67] found there was no epitaxy between the diboride and the Al matrix, then speculated that the effect of boron was to decrease the solubility of Ti in liquid Al and thus increase the number density and enhance dispersion of nucleating Al_3Ti particles. Davies' findings were supported by Marcantonio and Mondolfo [66], who concluded that grain refinement was achieved by nucleation of Al on primary Al_3Ti crystals under equilibrium conditions, while grain refinement in alloys outside the Al_3Ti primary field was due to non-equilibrium conditions. They argued that better grain refinement by addition of boron to Al-Ti alloys was not due to nucleation of Al by boride particles, but was a consequence of the expanded primary Al_3Ti field at the lower Ti content by addition of B through reducing the solubility of Ti in liquid Al, which steepened the slope of the liquidus leading to the formation of many Al_3Ti particles as nucleation sites for α-Al. However, a number of researchers (e.g. Refs. [22,68]) investigated the Al-rich corner of the Al-Ti-B phase diagram and showed that boron had virtually no effect on the Al-Ti phase diagram. Jones and Pearson [22] experimentally demonstrated that sole TiB_2 particles added from a master alloy with nearly stoichiometric quantities of Ti and B gave little or no grain refinement for Al, but could achieve fine grain size when they were combined with extra Ti.

The hypernucleation theory proposed by Jones [69] suggests that Ti atoms in the melt segregate to the melt/TiB_2 interface and subsequently promote the formation of a pseudo-crystal with a structure similar to that of α-Al. This theory was supported by subsequent work by Donnelly *et al.* [70] and Oh

et al. [71] who studied the interfaces of liquid Xe/α-Al and liquid Al/α-Al_2O_3 using high-resolution transmission electron microscopy (HRTEM), respectively, and by Men and Fan [72] who found that there exists a two-dimensional (2D) ordered structure at the liquid/substrate interface at temperatures above the liquidus using molecular dynamics (MD) simulation.

The duplex nucleation theory was proposed by Mohanty and Gruzleski [73], who suggested that Ti segregation to the melt/TiB_2 interface could reach such a level that the formation of Al_3Ti would be favoured, implying that the Ti content in the melt close to the interface would exceed 0.15wt.% to allow the peritectic reaction to taking place. This concept was dismissed by Sigworth [74] using a thermodynamic argument. In order to study the TiB_2/Al interface, Schumacher *et al.* [75,76] produced an amorphous Al alloy containing TiB_2 particles using a melt spinning technique, and found that there existed a 3nm thick crystalline phase with lattice spacing close to that of Al_3Ti phase between TiB_2 and the amorphous Al. However, it was difficult to precisely identify the Al_3Ti phase in their work. It is possible that the 3 nm crystal layer on the TiB_2 surface is α-Al formed in the solid state since the amorphous alloy is highly metastable and crystallization may take place heterogeneously on the TiB_2 surface.

Computer simulation techniques provide an alternative approach to direct experimental observations, which has been proven to be very difficult if possible at all since nucleation in metallic systems occurs at high temperature, small length scale and an extremely short period of time. From the density functional theory (DFT) simulation, Han *et al*. [77] found that an Al_3Ti-like thin layer could be thermodynamically stable on the TiB_2 surface prior to the solidification of Al. This finding was supported by Qin and Fan [78] who used the MD simulation to confirm that an atomic monolayer of (112) Al_3Ti two-dimensional compound (2DC) could be stable at the liquid Al/TiB_2 interface at temperatures above the melting point of Al. Eventually, Fan *et al.* [3] experimentally confirmed the hypothesis using high-resolution electron microscopy, and they found that there was a Ti-rich atomic monolayer on the (0001) TiB_2 surface, which is most likely to be a (112) Al_3Ti 2DC.

It is well accepted that the TiB_2 particles themselves are not effective for grain refinement of Al-alloys, while addition of excess Ti in the Al-Ti-B series of grain refiner can lead to remarkable grain refinement [1,14]. However, the exact mechanism for grain refinement by the Al-Ti-B grain refiner was only made clear very recently by Fan *et al.* [3]. They clearly showed the role of nucleant particle and the effect of solute Ti in Al-Ti-B series of grain refiners: (i) the TiB_2 particles with an Al_3Ti 2DC on its surface act as the nucleant particles due to the significant decrease in lattice misfit from -4.2% between the TiB_2 and α-Al to 0.09% between Al_3Ti and α-Al; (ii) a more important effect of Ti on grain refinement is to ensure the formation of Al_3Ti 2DC on the TiB_2 surface than just providing growth restriction.

2.2 Peritectic theory

The available experimental results suggest that the addition of peritectic elements usually reduces grain size more effectively than addition of eutectic elements. This is explained by the peritectic theory proposed by Crossley and Mondolfo [61], who experimentally investigated the effect of solutes on grain refinement through the addition of a small amount of Fe, Ti, Mo, Zr, W, and Cr to HP-Al. They found that significant grain refinement could be achieved by addition of peritectic formation elements, such as Ti, Mo, Zr, W, and Cr. Therefore, they proposed that such significant grain refinement was delivered by the formation of nucleant particles through the peritectic reaction. Marcantonio and Mondolfo [66] supported the hypothesis that the Al_3Ti phase acts as the nuclei for nucleation of α-Al during solidification of Al-alloys with Al-Ti-B addition, and they proposed that boron expands the field of primary crystallization of Al_3Ti resulting in the formation of Al_3Ti at low Ti contents (i.e., less than peritectic point (C_m) in Fig. 3a). However, later research work [22,68] revealed that boron addition had little impact on the primary field of Al_3Ti in Al-Ti-B alloys, although

solid particles formed through peritectic reaction can indeed refine grain size if there is a sufficient number density of such particles. Wang *et al.* [28] systematically investigated the effect of addition of eutectic-formers (Cu, Mg, Si) and peritectic-formers (V, Zr, Nb, Ti) on grain refinement of Al-alloys, and they found that beyond C_m the peritectic reactants were commonly found to act as the heterogeneous nucleation sites leading to grain refinement.

This phenomenon is found not only in Al-alloys but also in other alloys, such as Mg- and Zn-based alloys. For example, when Zr is added to Al-free Mg-alloys, grain size is significantly reduced, where the undissolved Zr particles act as the nucleant particles for Mg [79]. Liu *et al.* [34,35] investigated the grain refining mechanism of Zn-alloys with Ag and Cu addition, and they found an unusual trend of grain size: within C_m grain size decreased with increasing solute content; however, beyond C_m, grain size slightly increased. This might be caused by the formation of a new phase after C_m, e.g. $AgZn_3$ with Ag addition, which could act as the nucleant particle. Moreover, further addition of peritectic-formers, i.e. Ag and Cu in Zn alloys, made the primary particles larger leading to a reduced particle number density and eventually increased grain size. Peng *et al.* [80] investigated systematically the grain refining mechanism of Zr in commercial purity Mg (CP-Mg) with and without intensive melt shearing prior to solidification. Their results clearly demonstrated that there was a competition for nucleation between the exogenous Zr particles and the endogenous MgO particles, as will be introduced in more detail in Section 3.2.

2.3 Growth restriction of solute

It is well accepted that the solute accumulated/depleted ahead of the solid/liquid interface reduces the growth velocity during the diffusion-controlled growth process, which is termed as the growth restriction effect of solutes. Although solute growth restriction was attended as early as 1949 by Cibula [59], there has been no effective methodology to quantify the effect of growth restriction on grain size. Tarshis *et al.* [21] examined experimentally the solute effect on grain size in Ni- and Al-alloys with grain refiner addition. Based on their experimental results they proposed a constitutional supercooling parameter, P, to quantify the solute effect on grain size [21]:

$$P = \frac{mC_0(k-1)}{k}, \tag{1}$$

where m is the slope of the liquidus, C_0 is the solute concentration, and k is the partition coefficient, with these and other relevant parameters being illustrated in Figs. 3a and b. They demonstrated a clear correlation between grain size and P in Ni- and Al-alloys: when $P < 10$, the cast structure is essentially coarse (columnar), and the grain size decreases markedly with increasing P; when $P > 10$ the grain structure is predominantly equiaxed and the grain size decreases with increasing P but with a reduced decreasing rate. Spittle and Sadli [23] used the parameter P to analyse their experimental results of grain size of high purity Al-alloys with and without 0.2wt.% addition of Al-5Ti-1B grain refiner, and suggested that there appeared to be a good correlation between grain size and the parameter P.

Compared with P, the growth restriction factor, Q, is a much more popular parameter used to quantify the solute effect on grain size. Maxwell and Hollowell [44] are the first to introduce the term, $mC_0(k-1)$, to quantify the solute growth restriction for spherical growth during solidification. Thereafter, this term appeared in the modelling work by Hunt [81] and by Kurz *et al.* [82] to describe dendritic growth and many other modelling works to quantify the solute effect on grain size [e.g, 45-51]. Johnsson [24] studied experimentally the effect of solutes, such as Fe, Si and Ti, on the grain size of Al-alloys with addition of Al-5Ti-1B grain refiner using a two-thermocouple thermal analytical technique. Johnsson [24] named the term $mC_0(k-1)$ as growth restriction factor (GRF, designated as Q), and pointed out that, during diffusion-controlled growth, the grain size was inversely proportional to GRF:

$$Q = mC_0(k-1)\ . \tag{2}$$

Meanwhile, Johnsson [24] also proposed that for low concentration the growth restriction factor in a multi-component system (Q_m) could be obtained by using data from the constituent binary phase diagrams:

$$Q_m = \sum m_i C_{i0}(k_i - 1) = \sum Q_i, \tag{3}$$

where i is the ith solute in multi-component alloys.

Hodaj and Durand [83] proposed a new parameter, U, to account for the effect of kinetics on growth restriction factor, which is effectively a diffusion coefficient weighted growth restriction factor:

$$U = D_L \sum \frac{1}{D_i} m_i C_{0i}(k_i - 1) = D_L \sum \frac{1}{D_i} Q_i, \tag{4}$$

where D_L is the self-diffusion coefficient of the solvent, D_i is the diffusion coefficient of the ith solute. They showed that the correlation between grain number density and U was better than that proposed by Desnain *et al.* [84]. In Eq. (4) the contributions of the constituent solutes are weighted inversely by their diffusivities D_i. However, it is usually difficult to obtain reliable data for solute diffusivities in liquid alloys, and therefore, it is a common practice to use a constant diffusion coefficient for all the solutes during numerical modelling of solidification processes.

In order to describe Q more accurately, more efforts have been dedicated to obtaining more accurate values of Q in multicomponent alloys [85-88]. However, the validity of Q for quantifying the growth restriction of solute was challenged by Fan *et al.* [89], who proposed a new growth restriction parameter, β, and demonstrated clearly that for multicomponent systems, β is additive and Q is not. From theoretical analysis and phase-field simulations, Fan *et al.* [89] had confirmed that growth velocity was a unique function of β regardless of the nature of solutes, solute concentrations and solidification conditions, as will be described in more details in Section 3.3.

Easton and StJohn [29] investigated the effect of solute and nucleant particles on grain size and pointed out that both solute and nucleant particles play important role in grain refinement. They suggested that a particular value of GRF did not correlate with grain size for different solute types, even considering the presence of nucleant particles, and that grain size was dependent on the degree of the constitutional undercooling set by the composition, thermal profiles in the liquid ahead of the growing grain and the special distribution of the potent nucleant particles. Later, Lee *et al.* [30] studied the solute effect on grain refinement in Mg-alloys and concluded that the addition of certain solute elements to Mg led to a decrease in grain size and small additions had the greatest effect with grain size reaching a relatively constant value at higher levels. They also pointed out that: (1) the addition of a small amount of Al, Zr, Ca or Si produced a strong grain refining effect in pure magnesium because of the growth restriction effect; and (2) the effect of Zr seemed to be caused by both growth restriction effect and the introduction of nucleant particles. However, when grain size was plotted against GRF for Al, Zr, Ca, and Si, they found that grain size was not a unique function of GRF, which was interpreted as a consequence of the formation of nucleant particles due to the solute addition [30]. In addition, Chai *et al.* [90] used both experimental and theoretical approaches to evaluate the solute effect on grain size in Al-alloys, and they suggested that grain size was inversely proportional to Q for a given alloy with solute concentration below the solid solubility limit.

From the analysis of experimental data of Al alloys with additions of grain refiners, Easton and StJohn [47] proposed that the average grain size ($\bar{d}$) is proportional to the inverse of Q, i.e. $\bar{d} = a + b/Q$, where coefficient a is related to the maximum density of active TiB_2 nucleant particles in the melt, while coefficient b is related to the nucleation potency. A similar analysis is also conducted for Mg-

alloys [79]. StJohn *et al.* [79] analysed grain refinement by addition of Zr in Mg-alloys considering the variant of dissolved Zr in Mg melt and undissolved Zr particles with increasing Zr content. It should be realised that Zr addition even below the peritectic composition (C_m, 0.45wt.%Zr) may lead to undissolved Zr particles, which can act as nucleant sites during solidification. Zr addition increases not only Zr content in the melt but also the number density of undissolved Zr particles, with both contributing to grain refinement.

Most subsequent studies substantiated this linear relationship between grain size and $1/Q$, not only in Al- and Mg-alloys [28,31,32,91-94], but also in other alloys, such as Ti-alloys [37-39]. However, Becerra and Pekguleryuz [18] found experimentally that grain size of Mg-In alloys was better described as a function of $(1/Q)^{1/3}$. Similarly, Balart *et al.* [43] found that columnar grain length of Cu-alloys containing P, Mg, Mn, Pb, and Sn solidified at a constant degree of superheat fitted better with $(1/Q)^{1/3}$ than with $1/Q$.

Xu *et al.* [27] investigated experimentally the effect of solute elements (Cu and Zn) on grain refinement in Al-based hypoeutectic alloys. Grain size data of the as-cast structures were plotted against the values of P, Q, and, ΔT, which showed that the relationships between grain size and P or Q were complex, but grain size decreased monotonically with increasing ΔT over the whole range of the hypoeutectic compositions. This conclusion was further confirmed by Birol [95], who measured grain size of Al-Si and Al-Cu binary alloys with a large concentration range (up to 7wt.%), and found that ΔT was inversely related to the measured grain size and produced a closer correlation than GRF for the entire range of hypoeutectic solute concentrations. A similar conclusion was obtained earlier by Abdel-Reihim *et al.* [96], who studied the grain refinement of the Al-Si and Pb-Sb alloy systems and suggested that the longest solidification time associated with the maximum solubility limit led to optimum grain refinement when other conditions were kept constant.

However, the experimental results in Zn alloys show that the relationship obtained from Al- and Mg-alloys is not applicable to Zn alloys [33]. Liu *et al.* [33] studied the grain refinement of Zn alloys with both peritectic-forming elements (Cu and Ag) and eutectic-forming elements (Mg and Al). They found that although these four alloying elements all led to effective grain refinement of Zn-alloys, eutectic-forming elements (Mg and Al) seemed to have better grain refining efficiency than peritectic-forming elements (Cu and Ag), which is different from that obtained from Al and Mg-alloys.

Although Tarshis *et al.* [21] were aware of the issue of columnar to equiaxed transition (CET) at approximately $P = 10$, subsequent researchers did not pay sufficient attention to such changes in microstructure when dealing with the relationship between grain size and solute contents. From Spittle and Sadli's work [23], it was found that the grain size of HP-Al could be reduced from 1200μm for HP-Al to 110μm with increasing solute content. However, 56ppm Ti was introduced to the alloy through addition of 0.2wt.% of Al-5Ti-1B master alloy, which may compromise the conclusion from their work since Ti is considered to have a strong growth restriction. More importantly, in their work [23] the grain structure in the vertical section was not checked to eliminate potential samples with columnar grain structures. As pointed out by Fan *et al*. [3], an equiaxed grain structure in the cross-section is not sufficient to warrant an equiaxed grain structure in the as-cast sample, as schematically demonstrated in Fig. 4. This was also experimentally validated by Zhou *et al*. [56], who found that HP-Al with sufficient potent nucleant particles (up to $2.5\times10^{14}m^{-3}$) was still columnar structure rather than equiaxed without the presence of sufficient solute elements.

Another issue with many current research works is that the nature of nucleant particles is not clearly identified and adequately quantified when investigating the solute effect on grain size, especially when comparing the peritectic-forming solutes. For example, Liu *et al.* [34,35] indicated that beyond C_m, the nucleant particles were $AgZn_3$ and $CuZn_4$ for Zn-Ag and Zn-Cu alloys, respectively, and that the size, size distribution and number density of the nucleant particles varied with increasing solute

contents. Furthermore, the nature of nucleant particles and their size, size distribution and number density are unclear when the solute contents are less than C_m. It is, therefore, not rigorous to compare directly the solute effect on grain size in different alloys.

For isothermal solidification, growth restriction of solute cannot directly affect grain size, but indirectly through affecting growth velocity to alter the maximum undercooling achievable at recalescence, which in turn determines the number of grain initiation events according to the free growth model [45]. Therefore, the effect of solute growth restriction on grain size is strongly dependant on the size, size distribution and number density of the nucleant particles, as well as solidification condition (i.e. cooling rate). Consequently, the solute growth restriction effect on grain size can only be compared for different solutes when other conditions are kept constant.

2.4 Prediction of grain size

Maxwell and Hollowell [44] developed a numerical model to predict grain number density (related to grain size) for isothermal solidification according to the classical heterogeneous nucleation theory, where the parameter $mC_0(k-1)$ was introduced for the first time to describe the effect of growth restriction on grain refinement. The Maxwell-Hollowell model [44] has become the foundation for the subsequent modelling work on predicting grain size of as-cast microstructure. Spittle and Brown [97] simulated the solidification process of small castings using the Monte Carlo technique and revealed the relationship between P and grain size, which is consistent with the experimental results [21,23]. Desnain *et al.* [84] predicted numerically the grain number density in multi-component Al-alloys, and showed that minor solute additions could play an important role in determining grain size.

Another important advance in modelling grain refinement is the free growth model developed by Greer *et al.* [45]. Compared to the Maxwell-Hollowell model [44] where nucleant particles are assumed to have a mono-size, the free growth model assumes that nucleant particles have a size distribution. For the first time, the free growth undercooling (ΔT_{fg}) is related to the substrate size (d) through the following equation [45]:

$$\Delta T_{fg} = \frac{4\gamma}{\Delta S_v d}, \tag{5}$$

where γ is the interfacial energy of the solid/liquid interface, and ΔS_v is the entropy of fusion per unit volume. Eq. (5) suggests that: (1) the grain initiation is a deterministic process during solidification; (2) only the nucleated particles whose free growth undercooling is smaller than the undercooling of the melt can initiate grains; and (3) the largest nucleant particle(s) will initiate grain first, then followed by grain initiations with progressively smaller ones with decreasing temperature. Based on this principle, a numerical model was developed by Greer *et al.* [45] to predict grain size as a function of grain refiner addition level, cooling rate and alloy composition. In this model, Q was used to quantify the growth restriction of solute during solidification, and it was suggested that grain size was better described as a function of Q rather than P. Subsequently, Quested and Greer [98] proposed the concept of athermal nucleation on the basis of free growth model, and revealed the deterministic nature of grain initiation during solidification. In addition, Quested and Greer [99] applied the free growth model to analyse the performance of Al-5Ti-1B grain refiner for grain refining Al-alloys, and they concluded that although the existing commercial refiners are highly effective, they are very inefficient, with only less than 1% of the TiB_2 particles being active for grain initiation.

For a more explicit assessment of the solute effect on grain refinement, a new term, relative grain size (RGS), was proposed by Easton and StJohn [46]:

$$RGS = f_{sn} = 1 - \left(\frac{mC_0}{mC_0 - \Delta T_n}\right)^{1/P}, \tag{6}$$

where f_{sn} is the fraction solid when the constitutional undercooling, ΔT_c, reaches the undercooling required for nucleation, ΔT_n. For potent nucleants (ΔT_n is small), RGS is equivalent to $\Delta T_n/Q$ and therefore grain size is inversely proportional to Q. However, for impotent nucleant particles (i.e., ΔT_n is large), the accuracy of using Q to predict grain size will decrease. Meanwhile, Easton and StJohn [46] pointed out that the actual value of f_{sn} at ΔT_n calculated using Eq. (6) was more accurate than that from Q for predicting grain size when impotent nucleants were present. The same concept of RGS was also proposed later by Chen *et al.* [100] but with a different expression:

$$RGS = x_n = -\frac{D}{kv} ln \left|\frac{P-\Delta T_n}{P}\right|, \quad (7)$$

where v is the velocity of the solid-liquid interface, x_n is the solid growth distance at which the constitutional undercooling ΔT_c reaches the undercooling required for effective nucleation ΔT_n. Consistently, for potent nucleants, $\Delta T_n << P$, the RGS in Eq.(7) is substituted for RGS $\approx (D\Delta T_n)/(Qv)$ and RGS is therefore inversely proportional to Q; for impotent nucleants, grain size predicted using RGS is more appropriate than that from the parameter Q [100].

Same as in Maxwell and Hellawell model [44], the free growth model assumed isothermal solidification. However, during solidification, the solute enrichment/depletion ahead of the solid/liquid interface will form constitutional supercooling (CS) that is considered as a source creating the undercooling for nucleation in front of solid/liquid interface [18], particularly when there is a temperature gradient (e.g. directional solidification). Vandyoussefi and Greer [101] used cellular automaton-finite element (CA-FE) simulations to study grain refinement of directionally solidified Al-4.15wt.% Mg alloy with a temperature gradient. Nucleation of grains was described using an arbitrary Gaussian distribution which relates nuclei density ($dn/d\Delta T$) to undercooling and growth of grain was taken to be dendritic throughout. The CS effect of solute was not considered as the liquid composition outside the square envelopes of dendritic grains does not vary. This assumption is reasonable as the CS zone is only equivalent to a few times of the radius of the dendrite tip (only a few micrometres), which is much smaller than the radius of the dendritic grain and hence can be ignored. However, for spherical growth, the CS zone cannot be ignored. Quested and Greer [102] proposed a soft impingement mechanism of CS zones (about 2 times of the grain diameter) around the growing grains. They suggested that there would be no grain initiation event during the subsequent solidification once the CS zones of previously initiated grains overlap with each other. This soft impingement mechanism principally explains the reason for the low efficiency of grain refiner particles in the melt with large volume where there is no recalescence, and was used by Quested and Greer [102] to predict grain size in directional solidification with a particular temperature gradient.

Yao *et al.* [103] used a cellular automaton-finite control volume method (CAFVM) to investigate the effect of growth restriction and constitutional undercooling on grain size. They found that the effect of the GRF on grain refinement was more significant at low solute additions but was not evident with high solute contents, and they suggested that the significance of constitutional undercooling to grain refinement was most apparent at high solute levels. For additions of Ti (solute effects), extra nucleant particles will often accompany Ti additions due to its high reactivity with impurity elements (such as boron and carbon). The extra nucleant particles play a significant role in the grain refinement of Al [103]. Similarly, Qian *et al.* [49] developed an analytical model for CS-driven grain formation, which links the nucleation of new grains to the growth of a larger neighbouring grain. They pointed out that the average grain size was determined by two components: the minimum amount of growth that is needed to establish sufficient CS for nucleating the new grains; and the spatial mean distance from the advancing grain to the most potent nucleants available. Thereafter, the interdependence theory was developed by StJohn *et al.* [50], in which the final grain size is described as a function of three components: (i) the distance that a previously nucleated grain must grow in order to establish sufficient CS ahead of a solid/liquid interface to enable nucleation of the next grain; (ii) the distance from this S/L interface to the point where this critical amount of CS has been generated; and (iii) the

additional distance to the nearest most potent nucleant particle. In the interdependence theory, a nucleation free zone (NFZ) corresponding to CS zone was proposed to describe the fact that particles in the CS zone of a growing grain cannot initiate new grains due to lower undercooling. At the same time, SSNZ with the same meaning as NFZ was suggested by Shu *et al.* [52]. They developed a numerical model coupled with free growth model to predict the grain size of Al-alloys. They reported that the grain refinement of alloys of high solute content was controlled primarily by SSNZ. However, Du and Li [53] developed a numerical model based on the Kampmann-Wagner model and suggested that the SSNZ effect was negligible during isothermal solidification, where nucleation is ceased by the recalescence. The NFZ or SSNZ was later numerically analysed by Prasad *et al.* [104], and experimentally validated by Xu *et al.* [105, 106].

Most of the available models support the notion that grain size is proportional to $1/Q$. However, Men and Fan [51] developed an analytical model to account for the effect of solute elements on grain size. Their model suggests that grain size is related to the maximum undercooling, average growth velocity and solid fraction at the moment of recalescence, and thus is more accurately related to $(1/Q)^{1/3}$ for a given alloy system solidified under similar conditions.

Easton and StJohn [15] proposed two reasons why solute elements are essential for grain refinement: (1) solute partitioning restricts growth so that there is more time for more nucleation events to occur; and (2) the segregating elements lead to a CS zone in front of the solid/liquid interface, which activates the nucleants in front of the interface, interrupting the growth of the previous grain [107]. Under isothermal solidification condition, the mechanism of solute growth restriction on grain size can be described as that the solute elements in the liquid ahead of the growing crystals reduce the growth velocity of the initiated crystals and increase the maximum undercooling achievable before recalescence; this allows more particles to be active for grain initiation and, consequently, increases the number density of active particles, giving rise to a reduction of grain size.

More recently, it is realised that solidification of a single-phase alloy may involve a number of individual stages (Fig. 2), where nucleation and grain initiation are treated as two distinctly different processes [58]. Based on this concept, two distinct grain initiation modes have been identified depending on the interplay between nucleation undercooling (ΔT_n) and grain initiation undercooling of the largest nucleant particle ($\Delta T_{gi}(1st)$): progressive grain initiation (PGI) and explosive grain initiation (EGI) (see Fig. 5). PGI occurs when nucleation is relatively easy compared with grain initiation, i.e., $\Delta T_n < \Delta T_{gi}(1st)$. After nucleation, with further increase of undercooling first grain initiation occurs on the largest particle, and this is followed by grain initiation on progressively smaller particles until recalescence that stifles further grain initiation (see Fig. 5a). Progressive grain initiation results in a smooth cooling curve (Fig. 5c) and smooth variation of grain initiation rate with time (Fig. 5d). In contrast to PGI, EGI occurs when nucleation is relatively more difficult than grain initiation, i.e., at least $\Delta T_n > \Delta T_{gi}(1st)$. After nucleation, many particles that already satisfied the free growth criterion initiate grains almost simultaneously (Fig. 5b), leading to a sharp peak of grain initiation rate (Fig. 5d) and an abrupt rise of temperature in the cooling curve (Fig. 5c). It is important to point out that all nucleant particles nucleate the solid and develop solid caps on them with further decrease of melt temperature; however, only those nucleant particles that satisfied the free growth criterion before or at recalescence point will initiate grains and those failed to do so will have their caps dissolve back into the melt after recalescence (see Figs. 5a and 5b). Such grain initiation behaviour can be best described by grain initiation maps and grain refinement maps, which become very effective tools for assessing the effect of solute on grain refinement, as will be introduced in more details later in Section 3.5.5.

2.5 *In situ* observation of grain initiation

The recent development of powerful synchrotron source has made it possible to study grain formation during solidification *in situ* and in real-time [105,106, 108-113], including the formation of

intermetallic compounds (IMCs) [114-116]. It should be pointed out that the "nucleation" observed in Refs. [105,106, 109-113] should be taken precisely as grain initiation rather than nucleation. Due to the spatial resolution (about a few micrometers per pixel) and temporal resolution (a few tenths of a second) of the synchrotron X-ray experiment, it is impossible to observe the nano-scale nucleation process. [111-113]. As a result, grains can only be identified when they grow to about 10μm [112], which is much larger than the critical size for grain initiation. It was reported that grain initiation events appeared in waves in the inoculated melt under near isothermal solidification condition [109-112]. This burst of grain initiation events is speculated as the combination of SSNZ and inevitable small temperature gradient in the melt [110,111]. Interestingly, the burst of grain initiation events became weaker with decreasing solute content [113]. In contrast, there was no burst of grain initiation events observed in Al alloys without inoculation, where the grain initiation events occurred almost simultaneously in different regions of the melt [110]. This difference in grain initiation behaviour between inoculated and non-inoculated Al alloys was attributed to a much broader distribution of lower potency native nucleant particles in the non-inoculated alloys [110]. Although the interdependence theory [50] has been used to interpret such experimental observations [109,110,112], further investigations are required to validate the existence of burst of grain initiation and the exact mechanism for the observed non-uniform distribution of grain initiation.

3. Recent advances

3.1 Solute segregation at liquid/substrate interface

Solute segregation at the liquid/substrate interface is a wide-spread phenomenon driven by the reduction of the interfacial energy governed by the Gibb's adsorption rule [117-119]. The term "substrate" is defined here as any solid particle present in the melt that may act as a potential nucleation site, such as oxides, borides and carbides. The liquid/substrate interfacial energy is usually at the level of a few thousands of mJm^{-2}, and becomes a few hundreds of mJm^{-2} after adsorption of solute atoms. Consequently, such segregation is usually a monoatomic layer, only occasionally two or more layers [118,119]. As has realised by Cantor and his co-workers [120,121], such solute adsorption may play a critical role in the heterogeneous nucleation process. Depending on the chemical interaction between different type of atoms at the interface, solute segregation at the liquid/substrate interface may lead to different types of monolayers at the interface [57]:

- Formation of a 2-dimensional compound (2DC) at the liquid/substrate interface due to the chemical interaction between the solute and the solvent;
- Formation of a 2D random solid solution (2DS) between the solute and the solvent;
- Formation of a new surface layer on the substrate due to the chemical reaction between solute and substrate atoms;
- Dissolution of solute into the substrate to change the lattice parameter of the substrate.

Any such segregation will result in a change in the atomic arrangement at the liquid/substrate interface and hence the nucleation potency of the substrate, leading to an eventual change of as-cast grain size.

3.1.1 Change of lattice misfit

Prenucleation refers to atomic ordering in the liquid adjacent to the substrate/liquid interface at temperatures above the liquidus, which is manifested by both atomic layering vertical to the interface and in-plane atomic ordering parallel to the interface. In other words, prenucleation leads to the formation of a 2D ordered structure at liquid/substrate interface (see Fig. 6) [122]. It has been demonstrated by MD simulation that the formation of such 2D ordered structure is significantly enhanced by reducing the lattice misfit between the substrate and the solid [122], and reducing the

atomic level surface roughness [123]. In addition, DFT calculations showed that chemical interaction between the liquid atoms and the surface atoms of the substrate (measured by heat of mixing, ΔH_{mix}) can also influence the formation of the 2D ordered structures [124]; attractive interaction (negative ΔH_{mix}) enhances such ordering while repulsive interaction (positive ΔH_{mix}) impedes it [124]. However, it should be pointed out that such 2D ordered structure may lead to different consequences for the subsequent heterogeneous nucleation process; if the 2D ordered structure reduces lattice misfit it enhances heterogeneous nucleation, while if the ordered 2D structure increase lattice misfit it will impede heterogeneous nucleation [122]. The recent MD simulations [122, 125] revealed that the heterogeneous nucleation undercooling increases with increasing absolute values of misfit, no matter negative or positive it is. This suggests that the nucleation potency of a substrate can be manipulated by the segregation of solute atoms at the liquid/substrate interface.

One of the practical examples is Ti segregation at the liquid/TiB_2 interface. MD simulations [77,78] have suggested that an Al_3Ti-like thin layer could form on the TiB_2 surface, which is most likely due to the segregation of Ti in the melt. Fan *et al.* [3] experimentally observed the monoatomic layer of Al_3Ti 2DC, as shown in Fig. 7. Adsorption of Ti atoms at the liquid/TiB_2 interface leads to the formation of (112)Al_3Ti 2DC on the (0001)TiB_2 surface with the following orientation relationships:

$$(0\ 0\ 0\ 1)\ [1\ 1\ -2\ 0]TiB_2\ //\ (112)\ [-2\ 0\ 1]Al_3Ti//\ (1\ 1\ 1)\ [0\ -1\ 1]\ Al \quad (8)$$

The Al_3Ti 2DC reduces significantly the lattice misfit from -4.22% (between the TiB_2 terminal surface and the α-Al) to only 0.09% (between the Al_3Ti 2DC and the α-Al), making the TiB_2 with a monoatomic layer of Al_3Ti extremely potent for nucleating α-Al [3], providing potentially significant grain refinement.

However, not all solute segregations on the substrate surface could reduce the lattice misfit between the substrate and the solid. For example, when 500ppm of Zr is added in Al-alloys inoculated with Al-Ti-B grain refiner, the Al_3Ti 2DC on the TiB_2 becomes thermodynamically unstable and dissolves into the melt. Adsorption of Zr atoms at the liquid/TiB_2 interface leads to the formation of (0001)Ti_2Zr 2DC on the (0001)TiB_2 surface with the following orientation relationships [4]:

$$(0\ 0\ 0\ 1)\ [1\ 1\ -2\ 0]TiB_2\ //\ (0\ 0\ 0\ 1)\ [1\ 1\ -2\ 0]Ti_2Zr\ //\ (1\ 1\ 1)\ [0\ -1\ 1]\ Al \quad (9)$$

Formation of Ti_2Zr 2DC changes the lattice misfit back to -4.2% (between Ti_2Zr 2DC and α-Al), rendering TiB_2/Ti_2Zr particles impotent for nucleation of α-Al, and this phenomenon is referred to as Zr-poisoning as shown in Fig. 8 [4]. Another example of poisoning is addition of sufficiently high levels of Si. Wang *et al.* [10] studied the Si poisoning of Al-5Ti-1B grain refiner in Al-alloys with high contents of Si (>3wt.%). They showed that when Si was increased to a level of more than 3wt.%, the original Al_3Ti 2DC formed during the grain refiner production process became thermodynamically unstable and was gradually dissolved into the melt. The segregation layer was eventually replaced by a layer of Si-rich solid solution (denoted as 2DS), resulting in a reduced nucleation potency, as shown in Fig. 9 [10]. A similar conclusion was reported by Li *et al.* [126], who systematically investigated the Si poisoning and concluded that the segregation of Si atoms at the TiB_2/α-Al interface was likely the cause of Si poisoning.

3.1.2 Change of atomic level surface roughness

Using MD simulations, Jiang *et al.* [123] found that increasing atomic-level surface roughness of a crystalline substrate reduces both atomic layering and in-plane atomic ordering in the metallic liquid adjacent to the liquid/substrate interface. This suggests that heterogeneous nucleation can be impeded by roughening the substrate surface at atomic level. Similarly, Fang and Fan [127] investigated the interface between liquid Mg and octahedral MgO (denoted as MgO{1 1 1}) or cubic MgO (denoted as MgO{0 0 1}) using an *ab initio* molecular dynamics (AIMD) simulation technique. They

concluded that both MgO{1 1 1} and MgO{0 0 1} had an atomically rough surface in liquid Mg but for different reasons: MgO{1 1 1} becomes atomically rough due to the existence of vacancies in the terminating layer (see Figs. 10a-c), while MgO{0 0 1} becomes atomically rough because of the difference in bond length between Mg-O and Mg-Mg bonds (see Figs. 10d-f). In addition, Fang and Fan [128] also investigated the surface atomic arrangement of α-Al_2O_3{0 0 0 1} and MgO{1 1 1} in liquid Al using AIMD simulations. They found that α-Al_2O_3{0 0 0 1} became atomically rough due to the structural splitting of the terminating Al layer, while MgO{1 1 1} became atomically rough because of the existence of vacancies in the terminating Al layer. This atomically rough terminating layer deteriorates the atomic ordering in the liquid adjacent to the liquid/substrate interface, hence reduces the nucleation potency of the substrates.

A further example of the atomically rough surface due to interaction with the liquid is the segregation of Zr at the liquid Al/TiB_2 interface. As mentioned previously, segregation of Zr at the liquid Al/TiB_2 interface leads to the formation of a monolayer of (0 0 0 1) Ti_2Zr 2DC [4]. AIMD simulation has confirmed that as the new terminating surface layer of TiB_2, (0 0 0 1) Ti_2Zr 2DC is atomically rough since Zr atoms are considerably larger than Ti atoms (see Fig. 11). This means that Zr-poisoning is caused not only by the increased lattice misfit but more importantly by roughening the terminating surface of TiB_2, which is much more effective to hinder the structural templating power of the substrate.

Finally, it should be pointed out that an atomically rough surface of a substrate means higher interfacial energy between the liquid and the substrate, which in turn increases the tendency for segregation of solute elements at such interfaces due to the increased driving force.

3.1.3 Change of chemical potential

In addition to lattice misfit and atomic level surface roughness, the chemical interaction between the liquid and the substrate may also affect prenucleation. Fang *et al.* [124] used AIMD simulations to investigate systematically effect of substrate chemistry on atomic ordering in the liquid adjacent to the liquid/substrate interface. They found that for a given liquid metal, an attractive chemical interaction (negative heat of mixing) between the liquid and the substrate strengthens atomic ordering in the liquid at the interface, while a repulsive interaction (positive heat of mixing) weakens atomic ordering. Such a change in atomic ordering at the interface will alter the heterogeneous nucleation potency of the substrate, leading to a difference in the final grain size.

3.1.4 Composition templating

Usually, heterogeneous nucleation of IMCs is inherently more difficult than that of pure metal or a solid solution, because it requires not only the creation of a crystal structure but also the positioning of 2 or more types of elements in the lattice with specified compositions. Therefore, besides the structure templating, interfacial segregation of constituent elements may also facilitate heterogeneous nucleation, which is referred to as composition templating [129]. For instance, Que *et al.* [130] investigated experimentally heterogeneous nucleation of Fe-bearing IMCs in Al-alloys and found that the nucleation undercooling was a few tens of degrees, which is about an order of magnitude larger than that of a usual solid solution. After addition of modified TiB_2 (or AlB_2) particles with a layer of Fe-rich segregation in Al-Fe alloys, the α-$Al_{15}(Fe, Mn)_3Si_2$ was significantly refined, which is most likely due to the composition templating.

3.1.5 Dispersion of particles

Effective grain refinement requires sufficiently large number of particles to initiate grains. This means particle number density plays a crucial role in grain refinement. However, the particle number density may be altered by particle dissolution (e.g. Mg-Zr master alloy in Mg-alloys), settlement and

agglomeration of particles (e.g. TiB_2 in Al-alloys), particularly for these particles in sub-micro or nanometre size range.

Particle agglomeration is a wide-spread phenomenon in the field of metal matrix composites (MMCs) [131-135] where the nano- or micro-meter sized particles, e.g. SiC, Al_2O_3, or TiB_2, are used as reinforcement to improve the performance of MMCs. Taking the production of Al/TiB_2 MMC for example, Ti-containing and B-containing salts are added to the Al melt, resulting in a series of chemical reactions which produce sub-micron TiB_2 particles within the melt. Watson *et al.* [135] examined the TiB_2 cluster size and size distribution in CP-Al containing approximately 10wt.% TiB_2. They found that most of the TiB_2 clusters were larger than 10 μm, and these clusters had a log-normal size distribution, which was almost unchanged after held at high temperature (700 ^{0}C) for 4 hours. In addition, *in situ* observation of solidification of Al-Cu-alloys inoculated by Al-Ti-B grain refiner also confirmed the phenomenon of agglomeration of TiB_2 particles in the melt [136]. Although an explanation for the cause of clustering has yet to be agreed upon, it is proposed that reactant salts and/or oxide films may play an important role in the formation of strong TiB_2 particle clusters [137].

It is generally accepted that adsorption of solute at the liquid/particle interface reduces the interfacial energy, which in turn reduces the tendency for particle agglomeration, as demonstrated by the addition of Mg in Al-alloys [138]. Therefore, the adsorption of solute elements at the liquid/particle interface not only modifies the nucleation potency but also increases the total number density, rendering both factors important for grain refinement. Here we offer two examples of grain refinement by dispersing oxide particles through elemental segregation at the liquid/substrate interface.

Wang *et al.* [139] investigated the segregation of Ca atoms at the Mg/MgO interface and its effect on grain refinement of Mg-0.5Ca alloys using advanced analytical electron microscopy. They showed that there was an adsorption layer rich in Al, N and Ca on the {1 1 1} facets of MgO particles, with the lattice structure resembling the structure of MgO. This means that such interfacial segregation changes neither the lattice misfit between MgO and Mg nor the nucleation potency of MgO particles. Similarly, Y was also found to segregate at the Mg/MgO interface, forming Y_2O_3 layers with increasing Y content [140]. Adsorption of Y at the Mg/MgO interface delivers little changes in either lattice misfit or nucleation potency of MgO. The observed grain refinement by addition of either Ca or Y can be attributed, at least partially, to the dispersion of MgO particles caused by the reduction of interfacial energy due to elemental segregation of Ca or Y at the Mg/MgO interface.

3.2. Formation of primary particles

Solute element, either intentionally added as alloying elements or inevitably present as impurity elements, may lead to the formation of intermetallics as the primary phase during solidification. Such primary phase particles may act as nucleation sites for subsequent heterogeneous nucleation of α-Al as the major phase. Therefore, this may have a significant influence on grain refinement of the as-cast microstructure.

For instance, Li *et al.* [141] investigated the mechanism of enhanced heterogeneous nucleation of Al-Mg alloys with intensive melt shearing and showed that the 0.7wt.% Mg addition could change the dominant oxide particles from Al_2O_3 in CP-Al to $MgAl_2O_4$ in Al-Mg-alloys, which can act as the heterogeneous nucleant particle for α-Al. Lee *et al.* [30] examined experimentally the solute effect on the grain size of Mg-alloys and pointed out that, besides the growth restriction effect of solute, effect of nucleant particles, either introduced with the alloying additions (e.g. Zr in Mg-alloy) or as primary phase formed as a result of these additions (e.g. Al_3Ti in Al-Ti alloys), might enhance the grain refinement. This point of view is also supported by the experimental results of Ca addition in a twin-roll-cast Mg-3Al-1Zn alloy from Jiang *et al.* [142], who suggested that the grain refinement through addition of Ca in the AZ31 alloy was attributed to the enhanced heterogeneous nucleation on Al_2Ca particles natively formed in the melts. Another interesting result reported by Cao *et al.* [143]

is that high purity Mg-Al alloys have a naturally fine grain size compared to commercial purity alloys with the same basic compositions. They speculated that the natively formed Al_4C_3 particles acted as the nucleant sites, and Fe or Mn impurity in commercial purity alloys degraded the potency of Al_4C_3 by forming Al-C-Fe or Al-C-Mn ternary particles, which were considered to be less potent than Al_4C_3, therefore, leading to larger grain size for commercial purity Mg-Al alloys [143].

Formation of primary solid particles is also commonly found in peritectic alloy systems, where the primary particles formed in hyper-peritectic alloys may act as heterogeneous nucleation sites for the formation of α-Al through a peritectic reaction, resulting in potential grain refinement, and this has been referred to as peritectic reaction theory in the literature [61]. For instance, Wang *et al.* [28,144] found that beyond C_m intermetallics were commonly found in Al-alloys containing peritectic-forming elements, which may act as the heterogeneous nucleation sites for α-Al, while below C_m, the heterogeneous nucleant particles were possibly the native oxide particles. Similarly, Liu *et al.* [34,35] investigated the grain refining mechanism in Zn-alloys with Ag and Cu additions. They found that before C_m grain size decreased with increasing solute contents; however, after C_m, the grain size slightly increased. This may be caused by the formation of $AgZn_3$ with Ag addition, which can act as nucleant particles but has a low number density. However, the heterogeneous nucleant particles were not clearly identified in their studies [34,35]. Moreover, the size, size distribution and number density of the new phase $AgZn_3$ changes with different levels of Ag addition, making it impossible to compare grain size of alloys with different Ag contents.

Peng *et al.* [80] experimentally investigated the grain refining mechanism in Mg-Zr alloys with and without intensive melt shearing prior to solidification. They confirmed that both MgO and Zr could act as nucleant particles for α-Mg, but the nucleation potency of Zr for α-Mg (lattice misfit being 0.67%) is much higher than that of MgO (lattice misfit being 7.9%). Before C_m (0.45wt.% for Mg-Zr system), native MgO particles act as nucleant particles and the dissolved Zr provides growth restriction. Under this condition, impotent nucleant particles (MgO) with a large number density ($10^{17}m^{-3}$) lead to EGI dominant grain initiation, resulting in significant grain refinement. However, after C_m, undissolved Zr particles with a high nucleation potency but a low number density make the grain initiation process fully progressive, giving rise to a decreased total number of initiated grains at recalescence and hence an increased grain size. The observed complex pattern of grain size as a function of Zr concentration provides a clear demonstration of competition for nucleation between Zr and MgO particles [80].

3.3. Growth restriction parameter β

For diffusion-controlled spherical growth, the growth velocity V of a grain of radius r is given by the following equation [145,146]:

$$V = \frac{\lambda^2 D_i}{2r}, \tag{10}$$

where λ is a parameter related to the instantaneous undercooling. If $\lambda^2/2$ is taken as the growth coefficient, its inverse, $2/\lambda^2$, can be considered as the growth restriction coefficient. From the generalised analytical solution for spherical growth during isothermal solidification by Fan and Lu [147], one obtains the following exact solution for the growth restriction coefficient:

$$\frac{2}{\lambda^2} = \frac{1-\alpha}{\alpha(1+\sqrt{\alpha}+\alpha)}, \tag{11}$$

where $\alpha = (C_L - C_0)/(C_L - C_S)$ is the solute supersaturation defined by Zener [146] and is applicable to all the cases where $0 < \alpha < 1$.

From Eq. (11), one can calculate the growth restriction coefficient, $2/\lambda^2$, as a function of $Q/\Delta T$, as shown in Fig. 12a. It is clear from Fig. 12a that the growth restriction coefficient $2/\lambda^2$ is a function of Q, ΔT and k; and any of these parameters alone will not be adequate to describe growth restriction. In addition, Fig. 12a also provides clear theoretical reasoning for why Q is not additive for multicomponent systems.

Based on this analysis, Fan *et al.* [89] defined the growth restriction parameter, β, to quantify growth restriction of solute:

$$\beta = \frac{mC_0(k-1)}{\Delta T} - k. \quad (12)$$

As shown in Fig. 12b, $2/\lambda^2$ becomes a monotonically increasing function of β, being independent of the nature of solutes. Furthermore, Fig. 12b provides a theoretical justification for the additivity of β for multicomponent systems:

$$\beta = \sum_{i=1}^{n} \beta_i = \frac{f_L}{f_S}. \quad (13)$$

where f_L and f_S are the phase fractions of the liquid and the solid, respectively. Eq. (13) suggests that the physical meaning of β is the ratio of the liquid phase fraction, f_L, to the solid phase fraction, f_S. More importantly, Eq. (13) provides a thermodynamic approach to calculating the true β values of multicomponent systems using CALPHAD software and associated thermodynamic databases.

3.4. Effect of growth restriction on CET

The primary objective of grain refinement is to achieve CET [1]. Based on the front blocking mechanism for CET proposed by Hunt [81], CET occurs when the equiaxed grains formed at the solidification front can effectively block the growth of columnar dendrites. In Hunt's model, it is possible to examine the influence of parameters, such as alloy composition, nucleation undercooling (i.e. nucleation potency) and grain number density on CET through the CET map (a temperature gradient (G) vs. growth velocity (V) plot). Fig. 13 shows a calculated CET map for Al-Cu-alloys with a grain number density of 10^{11}m^{-3} based on Hunt's model [81]. Fig. 13 suggests that equiaxed grain structures are favoured by high growth velocity, high solute concentration and low temperature gradient.

Theoretically, for idealised isothermal solidification, the grain structure should be always equiaxed regardless of the presence of the solute. However, the actual solidification process, such as the standard TP-1 test [55], cannot be absolute isothermal, and a small temperature gradient is always present during solidification, resulting in a narrow transitional zone (dashed box in Fig. 13). Under such a quasi-isothermal condition, the as-cast structure is more likely to be either equiaxed or columnar. In this case, even a small amount of solute can change significantly the as-cast grain structure. For example, for a given solidification condition specified by fixed G and V (e.g. point A in Fig. 13), when the Cu content is 0.2wt.%, the structure is fully columnar; however, when the Cu content increases to 0.3wt.%, it becomes fully equiaxed. This is also demonstrated by our experimental results [56]. For TP-1 test sample inoculated with sufficient number density of potent TiB_2 particles, the structure of HP-Al is columnar, while the structure of CP-Al is fully equiaxed [56], suggesting that the very limited impurities (about 0.15-0.3wt.% mainly of Si and Fe) play a critical role for the formation of fully equiaxed structures.

According to Hunt's front blocking mechanism of CET, at CET, the randomly close-packed equiaxed grains form a coherent skeleton with an extended volume fraction $\emptyset_E$ being 0.63. The actual solid fraction, f_S, is given by [148],

$$f_S = 1 - \exp(-\emptyset_E). \quad (14)$$

From Eq. (13) [89] one has the following criterion for CET for solidification under a small temperature gradient:

$$\beta = 1.14. \quad \text{(when } G \rightarrow 0\text{)} \quad (15)$$

Thus, β = 1.14 can be used as a criterion for CET under quasi-isothermal conditions: β = 1.14 for CET; β > 1.14 for fully equiaxed grain structures; and β < 1.14 for fully columnar grain structures.

This criterion was validated by the experimental results with binary Al-alloys using standard TP-1 tests, as shown in Fig. 14, where the concentrations for CET predicted by β = 1.14 are in good agreement with that obtained by experiments. According to Fan *et al.* [89], β is equally applicable to multi-component systems, and hence β = 1.14 should be also applicable to multi-component systems as a criterion for CET. This is confirmed experimentally in the Al-Fe-Si (Fig. 15a) and Al-Fe-Cu (Fig. 15b) ternary systems. As shown in Fig. 15, the experimentally determined compositions for CET is closely located around the β = 1.14 line. However, it should be pointed out that β = 1.14 as a criterion for CET is only applicable to solidification conditions where the temperature gradient is very small, i.e. $G \rightarrow 0$.

3.5. Effect of solute on grain size

3.5.1. Accurate assessment of the solute effect on grain size

Grain refinement is a complex phenomenon involving many factors that are operational simultaneously, such as alloy compositions and the chemical and physical nature of nucleant particles, which may include crystal structure, morphology, surface termination, size, size distribution and number density of the nucleant particles. To assess the grain refining effect of a particular solute, all other parameters should be kept constant. Failure to do so will lead to inaccurate conclusions, as have frequently occurred in the literature so far, although it is experimentally difficult to isolate the effect of solute growth restriction from that of other variables.

We have identified a number of useful procedures to improve the accuracy of assessing the solute effect on grain size:

- *An excess-Ti-free grain refiner for Al-alloys*: As the most powerful element for growth restriction, slight variation in Ti content may cause a substantial change in grain size, particularly for dilute Al-Ti alloys. To eliminate the influence of excess Ti (possibly other impurity elements induced by the addition of grain refiners, such as Si and Fe), a new grain refiner alloy, Al-1.54TiB_2 [149], was produced by repeated dilution-filter-dilution of the commercial Al-5Ti-1B grain refiner using HP-Al. The resultant Al-1.54TiB_2 master alloy contains only Al_3Ti 2DC sheathed TiB_2 particles with other impurities being reduced to a few ppm.
- *Intensive melt shearing for Mg-alloys*: for Mg-alloys, an intensive melt shearing technique [150-154] was adopted to disperse MgO particles to ensure a consistent total number density in the Mg melt prior to solidification processing. The particle number density in the fully sheared melt is estimated to be $10^{17}m^{-3}$, compared with $10^{14}m^{-3}$ in the non-sheared melts [155].
- *TP-1 test to standardise solidification condition*: The standard Alcan TP-1 test [55] provides a quasi-isothermal solidification with a constant cooling rate (3.5K/s) at the centre of the sample for Al- and Mg- alloys. Adaptation of TP-1 test procedures ensures compatibility of experimental data between different investigators.
- *Checking microstructure in the vertical section* to ensure that grain size is measured only for equiaxed grain structures. This will avoid the inaccuracy introduced by the "grain size" data

measured from the columnar structures. As long as grain size is measured from 2D sections, grain size is only meaningful for equiaxed grain structures.

3.5.2. Experimental reassessment of solute effect on grain size

The authors have conducted experimental work to reassess the solute effect on the grain size of Al- and Mg-alloys by implementing the procedures presented in section 3.5.1. The key experimental results are shown in Table 1 and Fig. 16 for Al-alloys and in Table 2 and Fig. 17 for Mg-alloys. The original experimental results by Spittle and Sadli [23] suggest that the grain size of Al-alloys decreases dramatically from about 1200μm for CP-Al to about 110μm with increasing solute content. The alloys with large grain size (larger than 400μm) are mainly located in the region of $\beta < 1.14$ (see Fig. 16), suggesting that they may have a columnar grain structure. TP-1 tests on those alloys ($\beta < 1.14$) were repeated here strictly according to the experimental procedures described in Ref. [23] and confirmed that they all exhibit columnar structures on the vertical sections, as marked by the dashed red circles in Fig. 16. Therefore, these samples should be excluded for assessing the solute effect on grain size.

From the results in Figs. 16 and 17 the following conclusions can be drawn:

- The most significant effect of solute on the as-cast microstructure is to deliver CET at $\beta = 1.14$.
- The growth restriction effect on grain size is only moderately effective in dilute alloys with $1.14 < \beta < 15$, and grain size becomes almost constant when $\beta > 15$.
- The exaggerated conclusion in the literature that solute has a significant effect on grain size is caused by the inclusion of erroneous grain size data of dilute alloys that have a columnar grain structure.

3.5.3. Theoretical assessment of the solute effect on grain size

The numerical model by Fan *et al*. [58] was used to analyse the effect of solute on grain size. The grain size data for Al-Cu, Al-Fe and Al-Si alloys inoculated with Al-1.54TiB_2 grain refiner solidified under the exact same solidification conditions were calculated and the results are presented in Fig. 18 as a function of β, where the blue dashed line is the fitted trend according to the calculated grain size and the vertical line represents $\beta = 1.14$. The numerical model was presented in Ref. [58] and the parameters used in the numerical simulation are listed in Table 3. From Fig. 18, the calculated grain size decreases with increasing β when $\beta < 20$, and levels off when $\beta > 20$, being in good agreement with the experimental results for Al- and Mg-alloys in Figs. 16 and 17.

Solidification behaviours of Al-Cu alloys that contain the same nucleant particles with the same size distribution and number density were analysed to further understand the effect of solute on grain size. Fig. 19a shows the calculated cooling curves of Al-Cu-alloys with different Cu contents solidified at a cooling rate of 3.5K/s (TP-1 test). The maximum undercooling obtained at recalescence, ΔT_{max}, increases with increasing solute content (Fig. 19b). The calculated total number of grain initiation events (N_{gi}) and the final grain size ($\bar{d}$) are presented in Fig. 19c and Fig. 19d as a function of Cu content, respectively. The number of grain initiation events increases and the grain size decreases with increasing solute contents at low Cu concentrations, while such changes are much moderate at high Cu concentrations since grain size ($\bar{d}$) is related to N_{gi} through the following equation [45]:

$$\bar{d} = \frac{0.5}{(N_{gi})^{1/3}}. \quad (16)$$

Fig. 19 suggests that when all other parameters are kept constant, an increase in solute concentration slows down crystal growth due to solute growth restriction, which in turn increases the max undercooling achievable at recalescence and allows more nucleant particles to participate in grain

initiation, consequently resulting in an increased total number of grain initiation events and thus reduced grain size.

3.5.4. Growth restriction in the case of partitionless solidification

As described in Ref. [89], for a given binary alloy solidifying under a given undercooling (ΔT) there is a critical concentration (C^*), below which $\beta = 0$. Let $\beta = 0$, one obtains C^* from Eq. (12):

$$C^* = \frac{k\Delta T}{m(k-1)}. \quad (17)$$

Eq. (17) suggests that for a given alloy C^* is a function of undercooling ΔT; and C^* increases with increasing undercooling ΔT. As schematically illustrated in Fig. 20 for both eutectic and peritectic systems, C^* marks the solute concentration at which the solidification undercooling equals the freezing range of the alloy. For a given undercooling ΔT, when $C_0 < C^*$, solidification becomes partitionless (non-equilibrium solidification) and therefore there is no growth restriction ($\beta = 0$); whereas when $C_0 > C^*$, growth restriction increases with increasing C_0 as described by Eq. (12).

Similarly, one can work out the conditions for partitionless solidification of multicomponent systems. Let $\beta = 0$ in Eq. (13), one has [89]:

$$\Delta T = \sum_{i=1}^{n} P_i, \quad (18)$$

where P_i is the freezing range of the constituent binary systems in a multicomponent system. When $\sum_{i=1}^{n} P_i \leq \Delta T$, solidification becomes partitionless and there is no growth restriction; while when $\sum_{i=1}^{n} P_i > \Delta T$, the overall growth restriction is described by Eq. (13).

It is very likely that partitionless solidification occurs in most of the Al-Zr, Al-Mn and Al-Cr alloys examined in Ref [23] and Table 1, because the maximum freezing ranges of these alloys are very small, being about 0.2K for Al-Zr alloys, 0.6K for Al-Mn alloys and 0.8K for Al-Cr alloys for the composition range used [156], which are in the range of undercooling of the TP-1 test (about 0.5K).

3.5.5. Growth restriction in the case of explosive grain initiation (EGI)

Based on the concept of progressive and explosive grain initiations [58] (see Fig. 5), the grain imitation map was developed to describe the grain initiation behaviour under different conditions [58]. Fig. 21a shows a typical grain initiation map presented as a ΔT_n-C plot, showing three different zones: progressive zone, explosive zone and transitional zone. In general, explosive grain initiation is favoured by lower solute content (C), reduced nucleation potency (ΔT_n), decreased cooling rate and increased number density of nucleant particles [58]. The solute effect on grain size can be illustrated more readily in the grain refinement maps developed in Ref. [58], which is exemplified as a ΔT_n-C plot containing iso-grain-size lines in Fig. 21b, where the grain initiation is divided into PGI dominant and EGI dominant zones, which are delineated by a line that represent the solidification conditions where the number of EGI and PGI events are equal. In the EGI dominant zone, grain size is independent of solute contents as suggested by the vertical iso-grain-size lines, while in the PGI dominant zone, grain size decreases with increasing solute contents, as demonstrated more explicitly in Fig. 21c.

3.6. Grain initiation free zone (GIFZ)

Solute accumulated/depleted in front of the solid/liquid interface forms a CS zone, as schematically illustrated in Fig. 22a. The actual undercooling that a nucleant particle experiences within the CS zone is less than that outside the CS zone. This means that it is not possible to have any grain initiation event within the CS zone, and therefore we define the CS zone together with the corresponding solid

particle as grain initiation free zone (GIFZ) [157]. The GIFZ has also been referred to as the NFZ [50] and the SSNZ [52] in the literature. It should be noted that GIFZ is a better and more accurate concept than NFZ or SSNZ, since at the stage of grain initiation nucleation should have occurred earlier on all the potential particles [58].

The concept of GIFZ can be used to analyse the effect of agglomeration of nucleant particles (e.g. TiB_2) on grain refinement. Particle agglomeration in liquid is a common phenomenon, especially for these systems with the particle size of sub-micron or nanometre range. The degree of particle agglomeration is described by the nearest particle distance, H (see Fig. 22a), which has a log-normal distribution [157]:

$$n_H = \frac{1}{\sigma_H H\sqrt{2\pi}} \exp - \left(\frac{[\ln(H)-\ln(H_0)]^2}{2\sigma_H^2}\right), \quad (19)$$

where n_H is the number of nucleant particles with the nearest distance H, H_0 is the mean particle distance, and σ_H is the standard deviation. The smaller the H_0, the more severe the agglomeration of particles.

Another interesting concept is re-melting of growing solid particles (e.g. α-Al) [157]. As schematically illustrated in Fig. 22b, the overlap of the CS zones of two growing solid particles with the nearest distance S leads to re-melting of the smaller solid particle, which becomes thermodynamically unstable due to the reduced undercooling. Solid particle re-melting leads to a reduced number of grains at the end of solidification, resulting in increased grain size.

Compared with the nucleant particles that have a greater tendency to agglomeration in the liquid, the growing solid particles are distributed much more randomly in the melt. Therefore, for analysing the effect of solid particle re-melting on grain size, the nearest distance between growing solid particles, S (as shown in Fig. 22b), is assumed to have a Gaussian distribution [157]:

$$n_S = \frac{1}{\sigma_S\sqrt{2\pi}} \exp - \frac{1}{2}\left(\frac{S-S_0}{\sigma_S}\right), \quad (20)$$

where n_S is the number of solid particles with a separation distance S, S_0 is the mean separation distance, and σ_S is the standard deviation.

Based on the concepts of GIFZ and solid particle re-melting, the effect of agglomeration of nucleant particles and re-melting of solid particles on the final grain size was assessed by Gao and Fan [157] using a numerical model presented in Ref. [58]. For the numerical calculations of grain size [157], the thickness of CS is assumed to be 4.6 times of the size of the initiated solid particle itself, which is equivalent to a cut of the CS zone at 1% higher than the nominal liquid composition [50]. Gao and Fan [157] showed that neither GIFZ nor the solid particle re-melting had any effect on grain size if the nucleant particles are uniformly distributed throughout the melt, as shown in Fig. 23, agreeing well with the results from Du and Li [53]. However, by considering the agglomeration of nucleant particles, GIFZ has a significant influence on grain size, as shown in Fig. 23a. With increasing particle agglomeration (i.e., reducing H_0), grain size becomes larger. Without particle agglomeration the numerical model under-estimates grain size by about 50%; when H_0 = 5μm, the numerically calculated grain size data agree well with experimental data [23] and this work (see Fig. 23a). In addition, the nucleant particles agglomeration does not affect the re-melting (see Fig. 23b) because the initiated solid particles are distributed much more uniformly throughout the melt. Furthermore, the numerical calculations showed that particle re-melting had little effect on grain size (see Fig. 23b) and hence could be omitted during the theoretical analysis of the solute effect on grain size [157].

4. Summary and perspective

In this paper, we have briefly reviewed the historical research on the solute effect on grain refinement of metallic materials. Although extensive research has been done on the subject and significant progress has been made over the past decades, such historical research is yet to deliver the desirable understanding of the solute effect on grain refinement; many key questions remain open, such as: how significant is growth restriction to grain refinement? what are the exact mechanisms of grain refinement? how to control heterogeneous nucleation to deliver more effective grain refinement? and many more. Our review of the historical research has identified a number of factors that have hindered progress in the past, and need to be addressed in future research:

- *Technically*, following the procedures of TP-1 tests, particularly assessing grain size on the central part of a specified cross-section alone, has led to the overestimate of solute effect on grain refinement particularly at low solute concentrations due to the inclusion of columnar grain data that are ill-defined and usually much larger than equiaxed grain size (Figs. 4 and 16.)
- *Analytically*, although the growth restriction factor, Q, has been widely used to assess the solute effect on grain refinement, it is not a unique function of growth restriction coefficient, $2/\lambda^2$, (Fig. 12a). In particular, Q is only marginally applicable to binary eutectic systems, but will cause more severe errors when applied to binary peritectic systems and multicomponent systems.
- *Theoretically*, models for predicting the effect of solute on grain size consider mainly effect of CS zone but with little or no consideration of the effect of nucleant particles, particularly in cases of no grain refiner addition, where the chemical nature of nucleant particles is often not identified without mentioning the specifications of critical physical characteristics, such as size, size distribution and number density of nucleant particles.
- *Practically*, research, development and industrial applications of grain refiners failed to consider the competition for nucleation between exogenous particles (e.g., TiB_2) and the endogenous particle, such as oxides, carbides, and nitrides. This has often led to ambiguous or even erroneous conclusions.

Following the brief review of the historical research, we examined holistically the solute effect on grain refinement and presented an overview of the recent advances on the subject:

- Segregation of solute elements at the liquid/substrate interface, either intentionally added as alloying elements or inevitably existed in the melt as impurity elements, may alter the potency and/or number density of nucleant particles, and consequently the final grain size.
- Solute addition may lead to the formation of primary solid particles (usually intermetallic compounds, or IMCs) that have the potential to dominate both heterogeneous nucleation and grain initiation processes, making the intended nucleant particles redundant for grain refinement.
- A critical role of solute is to deliver CET, which is the primary purpose of grain refinement. Under quasi-isothermal solidification condition, CET occurs at $\beta = 1.14$.
- After CET, the growth restriction parameter, β, is better than any other parameters for assessing the effect of solute on grain size, and is rigorously applicable to multicomponent alloy systems.
- Growth restriction of solute during crystal growth only has a moderate effect on grain size, being much less than the historical belief.
- Below a critical solute concentration, solidification becomes partitionless and there is no growth restriction.
- In the PGI dominant zone grain size decreases with increasing solute contents, while in the EGI dominant zone, solute has no effect on grain size.
- Promoting explosive grain imitation using impotent particles (large ΔT_n) will lead to more significant grain refinement (assuming no other more potent particle of significance present

in the melt) compared with enhancing progressive grain initiation with potent nucleant particles (small ΔT_n).

Review of the historical research and a holistic assessment of recent advances on solute effect on grain refinement has allowed the identification of a few areas for future research, which may have the potential to deliver more significant advance in both scientific understanding and industrial practice in the area of grain refinement:

- *Manipulation of nucleation potency* by intended segregation of selected minor alloying elements at the liquid/particle interface may lead to the development of new grain refiners, or identification of self-grain-refining alloys. This requires a new understanding of elemental selection for interfacial segregation, atomic arrangement of segregated atoms at the interface and the effect of such interfacial atomic structure on heterogeneous nucleation.
- *Dispersion of nucleant particles* can increase the number of grain initiation events leading to grain refinement. The approaches to particle dispersion can be either physical, such as the high shear melt conditioning technique [140-144], or chemical through elemental segregation at the liquid/particle interface to reduce interfacial energy [130].
- *Impeding heterogeneous nucleation* to deliver more significant grain refinement. Grain refinement is so far delivered mainly through enhancing heterogeneous nucleation (i.e. reducing ΔT_n). However, the concept of explosive grain initiation provides us with a more effective approach to grain refinement, i.e. increasing nucleation undercooling.
- *"Training" the native particles for grain refinement.* Repeated addition of grain refiners for grain refinement deteriorates the mechanical performance and makes recycling more difficult if possible. This problem is surmounted by making native particles available for effective grain refinement without the need of grain refiner addition.

Acknowledgements

Funding: This work has been funded by the EPSRC of the UKRI under the grant number EP/N007638/1.

References:

[1] McCartney DG. Grain refining of Al and its alloys using inoculants. Int Mater Rev 1989;34:247-60.
[2] Cantor B, Goringe MJ. (Eds.) Solidification and casting. The Institute of Physics, London, 2003.
[3] Fan Z, Wang Y, Zhang Y, Qin T, Zhou XR, Thompson GE, *et al.* Grain refining mechanism in the Al/Al-Ti-B system. Acta Mater 2015;84:292-304.
[4] Wang Y, Fang CM, Zhou L, Hashimoto T, Zhou X, Ramasse QM, Fan Z. Mechanism for Zr poisoning of Al-Ti-B based grain refiners. Acta Mater 2019;164:428-39.
[5] Jones GP, Pearson J. Factors affecting the grain-refinement of aluminium using titanium and boron additives. Metall Trans B 1976;7:223-34.
[6] Birch MEJ, Cowell AJJ. Grain refinement of aluminium alloys containing chromium and zirconium. Beech J, Jones H. (Eds.) Solidification Processing 1987, The Institute of Metals, London 1988; 149-52.
[7] Abdel-Hamid AA. Effect of other elements on the grain refinement of Al by Ti or Ti and B. Part I-A critical review. Z Metallkd 1989;80:566-69.
[8] Spittle JA, Sadli S. The influence of zirconium and chromium on the grain-refining efficiency of Al-Ti-B inoculants. Cast Metals 1995;8:247-53.

[9] Qiu D, Taylor JA, Zhang MX. Understanding the co-poisoning effect of Zr and Ti on the grain refinement of cast aluminium alloys. Metall Mater Trans A 2010;41:3412-21.
[10] Wang Y, Que ZP, Hashimoto T, Zhou X, Fan Z. Mechanism for Si poisoning of Al-Ti-B grain refiners in Al alloys. Metall Mater Trans A 2020;51:5743-57.
[11] Kori SA, Murty BS, Chakraborty M. Influence of silicon and magnesium on grain refinement in aluminium alloys. Mater Sci Technol 1999;15:986-92.
[12] Qiu D, Taylor JA, Zhang MX, Kelly PM. A mechanism for the poisoning effect of silicon on the grain refinement of Al-Si alloys. Acta Mater 2007;55:1447-56.
[13] Dong X, Ji S. Si poisoning and promotion on the microstructure and mechanical properties of Al-Si-Mg cast alloys. J Mater Sci 2018;53:7778-92.
[14] Murty BS, Kori SA, Chakraborty M. Grain refinement of aluminium and its alloys by heterogeneous nucleation and alloying. Inter Mater Rev 2002;47:3-29.
[15] Easton M, StJohn D. Grain refinement of Al alloys: part I. The nucleant and solute paradigms, A review of the literature. Metall Mater Trans A 1999;30:1613-23.
[16] Quested TE. Understanding mechanisms of grain refinement of Al alloys by inoculation. Mater Sci Technol 2004;20:1357-69.
[17] Greer AL. Overview: Application of heterogeneous nucleation in grain-refining of metals. J Chem Phys 2016;145:211704.
[18] Easton MA, Qian M, Prasad A, StJohn DH. Recent advances in grain refinement of light metals and alloys. Curr Opin Solid State Mater Sci 2016;20:13-24.
[19] Liu Z. Review of grain refinement of cast metals through inoculation: Theories and developments. Metall Mater Trans A 2017;48:4755-76.
[20] Easton MA, Prasad A, Qiu D, Gibson MA, Qian M, Brandt M, *et al.* Advances in grain refinement of light metals and alloys: An overview and some initial investigations into additive manufacturing. SP17-Solidification Processing 2017, Old Windsor, UK, July 2017;87-90.
[21] Tarshis LA, Walker JL, Rutter JW. Experiments on the solidification structure of alloy castings. Metall Trans 1971;2:2589-97.
[22] Jones GP, Pearson J. Factors affecting the grain-refinement of Al using Ti and boron additives. Metall Trans B 1976;7:223-34.
[23] Spittle JA, Sadli SB. Effect of alloy variables on grain refinement of binary Al alloys with Al-Ti-B. Mater Sci Technol 1995;11:533-37.
[24] Johnsson M. Grain refinement of Al studied by use of a thermal analytical technique. Thermochimica Acta 1995;256:107-21.
[25] Birch MEJ, Fisher P. in ‘Al Technology '86’, (ed. Sheppard T.) London, Institute of Metals 1986;117-24.
[26] Kori SA, Murty BS, Chakraborty M. Influence of Si and magnesium on grain refinement in Al alloys. Mater Sci Technol 1999;15:986-92.
[27] Xu H, Xu LD, Zhang SJ, Han Q. Effect of the alloy composition on the grain refinement of Al alloys. Script Mater 2006;54:2191-96.
[28] Wang F, Liu Z, Qiu D, Taylor JA, Easton MA, Zhang MX. Revisiting the role of peritectics in grain refinement of Al-alloys. Acta Mater 2013;61:360-70.
[29] Easton M, StJohn D. Grain refinement of Al alloys: part II Confirmation of, and a mechanism for, the solute paradigm. Metall Mater Trans A 1999;30:1625-33.
[30] Lee YC, Dahle AK, StJohn DH. The role of solute in grain refinement of magnesium. Metall Mater Trans A 2000;31:2895-906.
[31] Becerra A, Pekguleryuz M. Effects of zinc, lithium, and indium on grain size of magnesium. J Mater Res 2009;24:1722-29.
[32] Nagasekhar AV, Easton MA, Caceres CH. Solute content and the grain microstructure of high pressure diecast magnesium-Al alloys. Adv Eng Mater 2009;11:912-19.
[33] Liu Z, Wang F, Qiu D, Taylor JA, Zhang MX. Effect of solute elements on the grain refinement of cast Zn. Metall Mater Trans A 2013;44:4025-30.

[34] Liu Z, Qiu D, Wang F, Taylor JA, Zhang MX. The grain refining mechanism of cast zinc through silver inoculation. Acta Mater 2014;79:315-26.
[35] Liu Z, Qiu D, Wang F, Taylor JA, Zhang MX. Crystallography of grain refinement in cast zinc-copper alloys. J Appl Cryst 2015;48:890-900.
[36] Liu Z, Li R, Jiang R, Li X, Zhang MX. Effects of Al addition on the structure and mechanical properties of Zn alloys. J Alloys Comp 2016;687:885-92.
[37] Tamirisakandala S, Bhat RB, Tiley JS, Miracle DB. Grain refinement of cast Ti alloys via trace boron addition. Sci Mater 2005;53:1421-26.
[38] Bermingham MJ, McDonald SD, Dargusch MS, StJohn DH. The mechanism of grain refinement of Ti by silicon. Sci Mater 2008;58:1050-53.
[39] Bermingham MJ, McDonald SD, StJohn DH, Dargusch MS. Beryllium as a grain refiner in Ti alloys. J Alloys Comp 2009;481:L20-3.
[40] Balart MJ, Patel JB,Gao F, Fan Z. Grain refinement of deoxidized copper. Mater Trans A 2016;47:4988-5011.
[41] Cziegler AK, Schumacher P. Investigation of the correlation between growth restriction and grain size in Cu-alloys. Int J Cast Met Res 2017;30:251-5.
[42] Cziegler AK, Geraseva O, Schumacher P. Numerical and experimental investigation of the influence of growth restriction on grain size in binary Cu-alloys. Metals 2017;73:83.
[43] Balart MJ, GaoF, Patel JB, Miani F. Effects of superheat and solute Additions on grain size in binary copper alloys. Metall Micro Analy 2019;8:566-72.
[44] Maxwell I, Hellawell A. A simple model for grain refinement during solidification. Acta Metall 1975;23:229-37.
[45] Greer AL , Bunn AM, Tronche A, Evans PV, Bristow DJ. Modelling of inoculation of metallic melts: Application to grain refinement of Al by Al-Ti-B. Acta Mater 2000;48:2823-35.
[46] Easton MA, StJohn DH. A model of grain refinement incorporating alloy constitution and potency of heterogeneous nucleant particles. Acta Mater 2001;49:1867-78.
[47] Easton MA, StJohn DH. An analysis of the relationship between grain size, solute content, and the potency and number density of nucleant particles. Metall Mater Trans A 2005;36:1911-20.
[48] Easton MA, StJohn DH. Improved prediction of grain size of Al alloys that includes effect of cooling rate. Mater Sci Eng A 2008;486:8-13.
[49] Qian M, Cao P, Easton MA, McDonald SD, StJohn DH. An analytical model for constitutional supercooling-driven grain formation and grain size prediction. Acta Mater 2010;58:3262-70.
[50] StJohn DH, Qian M, Easton MA, Cao P. The interdependence theory: The relationship between grain formation and nucleant selection. Acta Mater 2011;59:4907-21.
[51] Men H, Fan Z. Effects of solute content on grain refinement in an isothermal melt. Acta Mater 2011;59:2704-12.
[52] Shu D, Sun B, Mi J, Grant PS. A quantitative study of solute diffusion field effects on heterogeneous nucleation and grain size of alloys. Acta Mater 2011;59:2135-44.
[53] Du Q, Li Y. An extension of the Kampmann-Wagner numerical model towards as-cast grain size prediction of multicomponent Al alloys. Acta Mater 2014;71:380-89.
[54] Wagner R, Kampmann R. Homogeneous second phase precipitation. In: Cahn RW, editor. Materials science and technology: a comprehensive treatment. Weinheim: John Wiley; 1991.
[55] Standard test procedure for Al alloy grain refiners (TP-1). Washington, DC: The Al Association; 1990.
[56] Zhou L, Gao F, Peng GS, Alba-Baena N. Effect of potent TiB_2 addition levels and impurities on the grain refinement of Al. J Alloys Comp 2016;689:401-7.
[57] Fan Z. An epitaxial model for heterogeneous nucleation on potent substrates. Metall Mater Trans A 2013;44:1409-18.
[58] Fan Z, Gao F, Jiang B, Que ZP. Impeding nucleation for more significant grain refinement. Scientific Report 2020;10:9448
[59] Cibula A. The mechanism of grain refinement of sand castings in Al alloys. J Inst Met 1949-50;76:321-60.

[60] Cibula A. The grain refinement of Al alloy castings by additions of Ti and boron. J Inst Met 1951-52;80:1-16.
[61] Crossley FA, Mondolfo LF. Mechanism of grain refinement in Al alloys. JOM 1951;3:1143-8.
[62] Mascre C,*et al.* Fonderie 1964;187:317
[63] Nakao Y. Preparation of A1-Ti-C master alloy through the addition of TiC to A1-Ti melts. Light Metals (Tokyo) 1967;17: 65-75.
[64] Seemann HJ, Staats H. The ultrasonic-dispersion of second phases in molten metals. Z Metallk 1968;59:347.
[65] Moriceau J. Germination of Al crystals with solidification by a Ti-boron compound. Compt Rend 1968;267C:231.
[66] Marcantonio JA, Mondolfo LF. Grain refinement in Al alloyed with Ti and Boron. Metall Trans 1971;2:465-71.
[67] Davies IG, Dennis JM, Hellawell A. The nucleation of Al grains in alloys of Al with Ti and boron. Metall Trans 1970;1:275-80.
[68] Sigworth GK. The grain refining of Al and phase relationships in the Al-Ti-B system. Metall Mater Trans A 1984;15:277-82.
[69] Jones GP. in: Beech J, Jones H (Eds), Solidification Processing, Sheffield: University of Sheffield 1987;496.
[70] Donnelly SE, Birtcher RC, Allen CW, Morrison I, Furuya K, Song M, *et al.* Ordering in a fluid inert gas confined by flat surfaces. Science 2002;296:507-10.
[71] Oh SH, Kauffmann Y, Scheu C, Kaplan WD, Ruhle M. Ordered liquid Al at the interface with sapphire. Science 2005;310:661-3.
[72] Men H, Fan Z. Atomic ordering in liquid Al induced by substrates with misfits. Comput Mater Sci 2014;85:1-7.
[73] Mohanty PS, Gruzleski JE. Mechanism of grain refinement in aluminium. Acta Mater 1995;43:2001-12.
[74] Sigworth GK. Communication on mechanism of grain refinement in aluminum. Scr Mater 1996;34:919-22.
[75] Schumacher P, Greer AL. Enhanced heterogeneous nucleation of α-Al in amorphous Al alloys. Mater Sci Eng A 1994;181:1335-9.
[76] Schumacher P, Greer AL, Worth J, Evans PV, Kearns MA, Fisher P, Green AH. New studies of nucleation mechanisms in Al alloys: Implications for grain refinement practice. Mater Sci Tech 1998;14:394-404.
[77] Han Y, Dai Y, Shu D, Wang J, Sun B. First-principles calculations on the stability of Al/TiB_2 interface. Appl Phys Lett 2006;89:144107.
[78] Qin T, Fan Z, IOP Conf Seri Mater Sci Eng 2011;27:012007.
[79] StJohn DH, Ma Q, Easton MA, Peng C, Hildebrand Z. Grain refinement of magnesium alloys. Metall Mater Trans A 2005;36:1669-79.
[80] Peng GS, Wang Y, Fan Z, Competitive heterogeneous nucleation between Zr and MgO particles in commercial purity magnesium. Metall Mater Trans A 2018;49:2182-92.
[81] Hunt J. Steady state columnar and equiaxed growth of dendrites and eutectic. Mater Sci Eng 1984;65:75-83.
[82] Kurz W, Giovanola B, Trivedi R. Theory of microstructural development during rapid solidification. Acta Metall 1986;34:823-30.
[83] Hodaj F, Durand F. Equiaxed grains in multicomponent alloys: Effect of growth rate. Acta Mater 1997;45:2121-7.
[84] Desnain P, Fautrelle Y, Meyer JL, Riquet JP, Durand F. Prediction of equiaxed grain density in multicomponent alloys. Acta metall 1990;38:1513-23.
[85] Quested TE, Greer AL, Analytical model linking growth restriction to solute interaction in model Al based ternary systems. Mater Sci Tech 2005;21:985-94.
[86] Quested TE, Greer AL. Thermodynamic modelling of growth-restriction effects in Al alloys. Acta Mater 2005;53:1323-34.

[87] Schmid-Fetzer R, Kozlov A. Thermodynamic aspects of grain growth restriction in multicomponent alloy solidification. Acta Mater 2011;59:6133-44.
[88] Mitrasinovica AM, Hernández FCR. Determination of the growth restriction factor and grain size for Al alloys by a quasi-binary equivalent method. Mater Sci Eng A 2012;540:63-9.
[89] Fan Z, Gao F, Zhou L, Lu SZ. A new concept of growth restriction. Acta Mater 2018;152:248-57.
[90] Chai G, Bäckerud L, Arnberg L. Relation between grain size and coherency parameters in Al alloys. Mater Sci Technol 1995;11:1099-103.
[91] Joshi U, HariBabu N. The grain refinement potency of bismuth in magnesium. J Alloys Comp 2017;695:971-5.
[92] Srivastava N, Chaudhari GP, Qian M. Grain refinement of binary Al-Si, Al-Cu and Al-Ni alloys by ultrasonication. J Mater Proc Tech 2017;249:367-78.
[93] Bazhenov VE, Magura MA. Effects of Si and Cu contents on grain size of Al-Si-Cu-alloys. Mater Sci Tech 2018;34:1287-94.
[94] Jing L, Lu T, Pan Y. Grain refining efficiency and the role of alloying elements in determining the nucleation potency of LaB6 in Al alloys. JOM 2020;72:3725-32.
[95] Birol Y. Effect of silicon content in grain refining hypoeutectic Al-Si foundry alloys with boron and titanium additions. Mater Sci Techn 2012;28:385-9.
[96] Abdel-Reihim M, Hess N, Reif W, Birch MEJ. Effect of solute content on the grain refinement of binary alloys. J Mater Sci 1987;22:213-8.
[97] Spittle JA, Brown SGR. Computer simulation of effects of alloy variables on the grain structures of castings. Acta metall 1989;37:1803-10.
[98] Quested TE, Greer AL. Athermal heterogeneous nucleation of solidification. Acta Mater 2005;53:2683-92.
[99] Quested TE, Greer AL. Effect of the size distribution of inoculant particles on as-cast grain size in Al alloys. Acta Mater 2004;52:3859-68.
[100] Chen Z, He Z, Jie W. A model for evaluation of grain sizes of Al alloys with grain refinement additions. J Mater Sci Technol 2007;23:619-22.
[101] Vandyoussefi M, Greer AL. Application of cellular automaton-finite element model to the grain refinement of directionally solidified Al-4.15wt.% Mg-alloys. Acta Mater 2002;50:1693-705.
[102] Quested TE, Greer AL. Grain refinement of Al-alloys: Mechanisms determining as-cast grain size in directional solidification. Acta Mater 2005;53:4643-53.
[103] Yao X, McDonald SD, Dahle AK, Davidson CJ, StJohn DH. Modeling of grain refinement: Part I Effect of the solute Ti for aluminum. J Mater Res 2008;23:1282-91.
[104] Prasad A, Yuan L, Lee PD, StJohn DH. The Interdependence model of grain nucleation: A numerical analysis of the Nucleation-Free Zone. Acta Mater 2013;61:5914-27.
[105] Xu Y, Casar D, Du Q, Mathiesen RH, Arnberg L, Li Y. Heterogeneous nucleation and grain growth of inoculated Al alloys: An integrated study by *in situ* X-radiography and numerical modelling. Acta Mater 2017;140:224-39.
[106] Xu Y, Casari D, Mathiesen RH, Li Y. Revealing the heterogeneous nucleation behavior of equiaxed grains of inoculated Al-alloys during directional solidification. Acta Mater 2018;149:312-25.
[107] Tøndel PA. PhD Thesis. The University of Trondheim. 1994.
[108] Nguyen-Thi H, Salvo L, Mathiesen RH, Arnberg L, Billia B, Suery M, Reinhart G. On the interest of synchrotron X-ray imaging for the study of solidification in metallic alloys. Comptes Rendus Physique 2012;13:237-45.
[109] Prasad A, Liotti E, McDonald SD, Nogita K, Yasuda H, Grant PS, StJohn DH. Real-time synchrotron x-ray observations of equiaxed solidification of aluminium alloys and implications for modelling. IOP Conf. Series: Mater Sci Eng 2015;84:012014.
[110] Prasad A, McDonald SD, Yasuda H, Nogita K, StJohn DH. A real-time synchrotron X-ray study of primary phase nucleation and formation in hypoeutectic Al-Si alloys. J Crystal Growth 2015;430:122-37.

[111] Liotti E, Arteta C, Zisserman A, Lui A, Lempitsky V, Grant PS. Crystal nucleation in metallic alloys using x-ray radiography and machine learning. Sci Adv 2018;4:eaar4004.
[112] Jia Y, Huang H, Fu Y, Zhu G, Shu D, Sun B, StJohn DH. An in situ investigation of the solute suppressed nucleation zone in an Al-15 wt% Cu alloy inoculated by Al-Ti-B. Script Mater 2019;167:6-10.
[113] Xu J, Li Y, Ma K, Fu Y, Guo E, Chen Z, Gu Q, Han Y, Wang T, Li Q. In-situ observation of grain refinement dynamics of hypoeutectic Al-Si alloy inoculated by Al-Ti-Nb-B alloy. Script Mater 2020;187:142-47.
[114] Yu JM, Wanderka N, Rack A, Daudin R, Boller E, Markötter H, Manzoni A, Vogel F, Arlt T, Manke I, Banhart J. Formation of intermetallic δ phase in Al-10Si-0.3Fe alloy investigated by in-situ 4D X-ray synchrotron tomography. Acta Mater 2017;129:194-202.
[115] Feng S, Liotti E, Lui A, Wilson MD, Connolley T, Mathiesen RH, Grant, PS. In-situ X-ray radiography of primary Fe-rich intermetallic compound formation. Acta Mater 2020;196:759-69.
[116] Song Z, Magdysyuk OV, Tang L, Sparks T, Cai B. Growth dynamics of faceted $Al_{13}Fe_4$ intermetallic revealed by high-speed synchrotron X-ray quantification. J Alloys Compounds 2021; 861:158604.
[117] Gibbs JW. The Collected Works of J. W. Gibbs Yale University Press, New Haven, 1948;1.
[118] Seah MP. Interface adsorption, embrittlement and fracture in metallurgy: A review. Surf Sci 1975;53:168-212.
[119] Kaplan WD, Chatain D, Wynblatt P, Carter WC. A review of wetting versus adsorption, complexions, and related phenomena: The rosetta stone of wetting. J Mater Sci 2013;48:5681-717.
[120] Cantor B. Heterogeneous nucleation and adsorption. Phil. Trans. R. Soc. Lond. A, 2003;361: 409-17.
[121] Kim WT, Cantor B. An adsorption model of the heterogeneous nucleation of solidification. Acta Metall Mater 1994;42:3115-27.
[122] Fan Z, H Men. A molecular dynamics study of heterogeneous nucleation in generic liquid/substrate systems with positive lattice misfit. Mater Res. Express 2020;7:126501.
[123] Jiang B, Men H, Fan Z. Atomic ordering in the liquid adjacent to an atomically rough solid surface. Comp Mater Sci 2018;153:73-81.
[124] Fang CM, Men H, Fan Z. Effect of substrate chemistry on prenucleation. Metall Mater Trans A 2018;49:6231-42.
[125] Fan Z, Men H, Wang Y, Que Z. A new atomistic mechanism for heterogeneous nucleation in the systems with negative lattice misfit: Creating a 2D template for crystal growth. Metals 2021;11:478.
[126] Li Y, Hu B, Liu B, Nie A, Gu Q, Wang J, Li Q. Insight into Si poisoning on grain refinement of Al-Si/Al-5Ti-B system. Acta Mater 2020;187:51-65.
[127] Fang CM, Fan Z. Prenucleation at the interface between MgO and liquid magnesium: An *ab initio* molecular dynamics study. Metall Mater Trans A 2020;51:788-97.
[128] Fang CM, Fan Z. Prenucleation at the liquid-Al/α-Al2O3 and the liquid-Al/MgO interfaces. Comp Mater Sci 2020;171:109258.
[129] Fan Z, Que ZP, Wang Y, Jiang B. Structural and compositional templating for heterogeneous nucleation, in "Frontier of solidification: Symposium in honour of Michel Rappaz, ed. W. Kurz *et al*., TMS, 2016.
[130] Que ZP, Zhou YP, Wang Y, Fan Z. Composition templating for heterogeneous nucleation of intermetallic compounds, SP17-Solidification Processing 2017, Old Windsor, UK, July 2017;158-61.
[131] Bakshi SR, Lahiri D, Agarwal A. Carbon nano tube reinforced metal matrix composites - a review. Int Mater Rev 2010;55:41-64.
[132] Lloyd DJ. Particle reinforced Al and magnesium matrix composites, Int Mater Rev 1994;39:1-23.

[133] Yashpal Y, Sumankant A, Jawalkar CS, Verma AS, Suri NM. Fabrication of Al metal matrix composites with particulate reinforcement: a review, Mater Tod: Proceedings 2017;4:2927-36.
[134] Sardar S, Karmakar SK, Das D. Ultrasonic assisted fabrication of magnesium matrix composites: A review. MaterTod: Proceedings 2017;4:3280-89.
[135] Watson IG, Forster MF, Lee PD, Dashwood RJ, Hamilton RW, Chirazi A. Investigation of the clustering behaviour of Ti diboride particles in aluminium. Compos: Part A 2005;36:1177-87.
[136] Jia Y, Wang D, Fu Y, Dong A, Zhu G, Shu D, Sun B. In situ investigation of the heterogeneous nucleation sequence in Al-15 weight percent Cu-alloy inoculated by Al-Ti-B. Metall Mater Trans A 2019;50:1795-804.
[137] Asbjornsson EJ. PhD thesis, University of Nottingham 2001.
[138] Kumar GSV, Murty BS, Chakraborty M. Grain refinement response of LM25 alloy towards Al-Ti-C and Al-Ti-B grain refiners. J Alloys Comp 2009;472:112-20.
[139] Wang SH , Wang F, Wang Y, Ramasse QM, Fan Z. Segregation of Ca at the Mg/MgO interface and its effect on grain refinement of Mg-alloys. IOP Conf Ser: Mater Sci Eng 2019;529:012048.
[140] Wang SH. PhD thesis. Brunel University London 2020.
[141] Li HT, Wang Y, Fan Z. Mechanisms of enhanced heterogeneous nucleation during solidification in binary Al-Mg-alloys. Acta Mater 2012;60:1528-37.
[142] Jiang B, Liu W, Qiu D, Zhang MX, Pan F. Grain refinement of Ca addition in a twin-roll-cast Mg-3Al-1Zn alloy. Mater Chem Phys 2012;133:611-6.
[143] Cao P, Qian M, StJohn DH. Native grain refinement of magnesium alloys. Script Mater 2005;53:841-4.
[144] Wang F, Qiu D, Liu Z, Taylor JA, Easton MA, Zhang MX. The grain refining mechanism of cast Al by zirconium. Acta Mater 2013;61:5636-45.
[145] Aaron HB, Fainstein D, Kotler GR. Diffusion-limited phase transformations: a comparison and critical evaluation of the mathematical approximations. J Appl Phys 1970;41:4404-10.
[146] Zener C. Theory of growth of spherical precipitates from solid solution. J Appl Phys 1949;20: 950-3.
[147] Fan Z, Lu SZ. A simple model for spherical growth in alloy solidification. IOP Conf Series: Mater Sci Eng 2016;117:012016.
[148] Christian JW. The theory of transformations in metals and alloys. Pergamon Press, Oxford, 2002.
[149] Zhou L, PhD thesis, Brunel University London 2015.
[150] Fan Z, Wang Y, Xia M, Arumuganathar S. Enhanced heterogeneous nucleation in AZ91D alloy by intensive melt shearing. Acta Mater 2009;57:4891-901.
[151] Fan Z, Jiang B, Zuo Y. Apparatus and method for liquid metals treatment, US 20130228045 A1, 2013
[152] Patel JB, Yang X, Mendis CL, Fan Z. Melt conditioning of light metals by application of high shear for improved microstructure and defect control. JOM 2017;69:1071-6.
[153] Fan Z, Zuo Y, Jiang B. A new technology for treating liquid metals with intensive melt shearing. Mater Sci Forum 2010:690:141-144.
[154] Zuo Y, Li H, Xia M, Jiang B, Scamans GM, Fan Z. Refining grain structure and porosity of an aluminium alloy with intensive melt shearing. Script Mater 2011;64:209-212.
[155] Men H, Jiang B, Fan Z. Mechanisms of grain refinement by intensive shearing of AZ91alloy melt. Acta Mater 2010;58:6526-34.
[156] The data are calculated using Pandat software with PanAl database.
[157] Gao F, Fan Z. Effect of nucleant particle agglomeration and solid particle re-melting on grain refinement, submitted.

Table 1 Summary of chemical compositions (in wt.%) and grain structures (TP-1 tests) of Al-alloys used in Fig.16.

Structure	Mg	Fe	Cu	Sn	Ti	Cr	Zr	Mn
Columnar	0.108	0.138	0.136	0.085	0.023	0.114	0.084	0.368
			0.25	0.197	0.051	0.206	0.142	0.557
				0.236	0.076	0.354	0.162	1.337
						0.47	0.32	1.737
Equiaxed	0.224	0.213	0.349	0.357	0.096			
	0.319	0.24	0.819	0.564				
	0.774	0.344	1.674					
	1.276							

Table 2 Summary of chemical compositions (in wt.%) and grain structures (TP-1 tests) of Mg-alloys used in Fig.17.

Structure	Al	Ca	Sn	Zn
Columnar	0.1	0.05	0.1	0.1
	0.3	0.1	0.4	0.3
Equiaxed	1	0.3	0.7	1
	3	0.5	1	3
	9	0.7	1.5	9
		1	2	

Table 3 Summary of values for the key parameters used in the numerical calculation of grain size presented in Fig. 18.

Parameters (symbol, unit)	Al-Si	Al-Cu	Al-Fe
Partition coefficient (k)	0.107 [89]	0.13 [89]	0.023 [89]
Liquidus slope (m, K(wt.%)$^{-1}$)	-5.805 [89]	-2.5 [89]	-3.184 [89]
Heat capacity (c_{pv}, Jm^{-3}K^{-1})		2.58×10^{6} [99]	
Enthalpy of fusion (ΔH_V, Jm^{-3})		9.5×10^{8} [99]	
Diffusion coefficient (D, m^{2}s^{-1})		2.52×10^{-9} [99]	
Gibbs-Thompson coefficient (Γ, Km)		1.42×10^{-7} [99]	
Log-normal distribution mean of particles (d_0, m)		0.68×10^{-6} [99]	
SD of log-normal distribution of particles (σ)		0.876 [99]	
Particle number density (N_0, m^{-3})		1×10^{13}	
Cooling rate (Ks^{-1})		3.5	

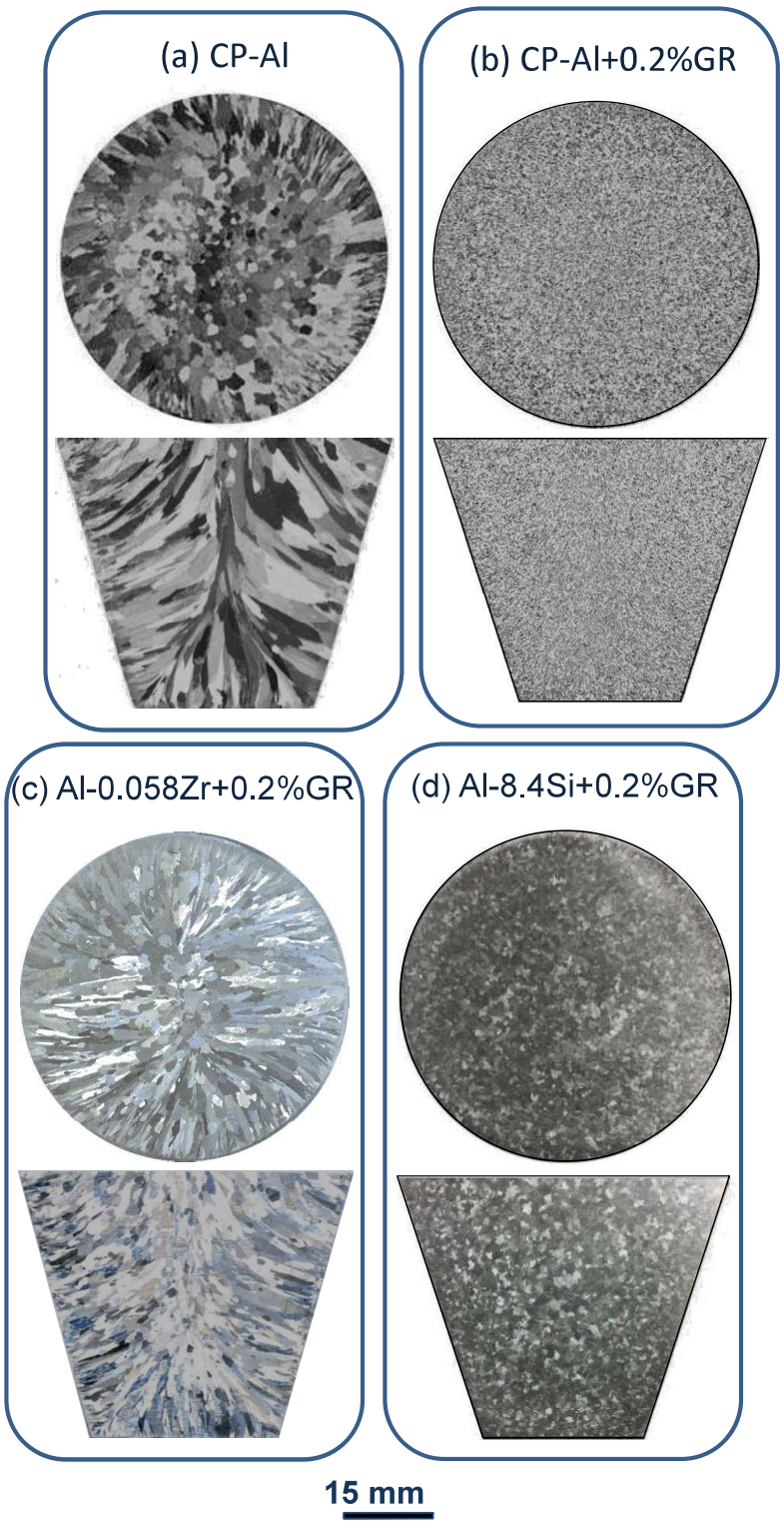

Fig. 1. Macrographs showing the grain structures of samples solidified in the TP-1 mould: (a) CP-Al without grain refiner (GR) showing a columnar grain structure [3]; (b) CP-Al with addition of 0.2% commercial Al-5Ti-1B grain refiner showing a fine and equiaxed grain structure [3]; (c) CP-Al with the minor addition of Zr (0.058%) and 0.2% commercial Al-5Ti-1B grain refiner showing a columnar grain structure [4]; (d) Al-8.4Si alloys with 0.2% commercial Al-5Ti-1B grain refiner showing a coarse equiaxed grain structure [10].

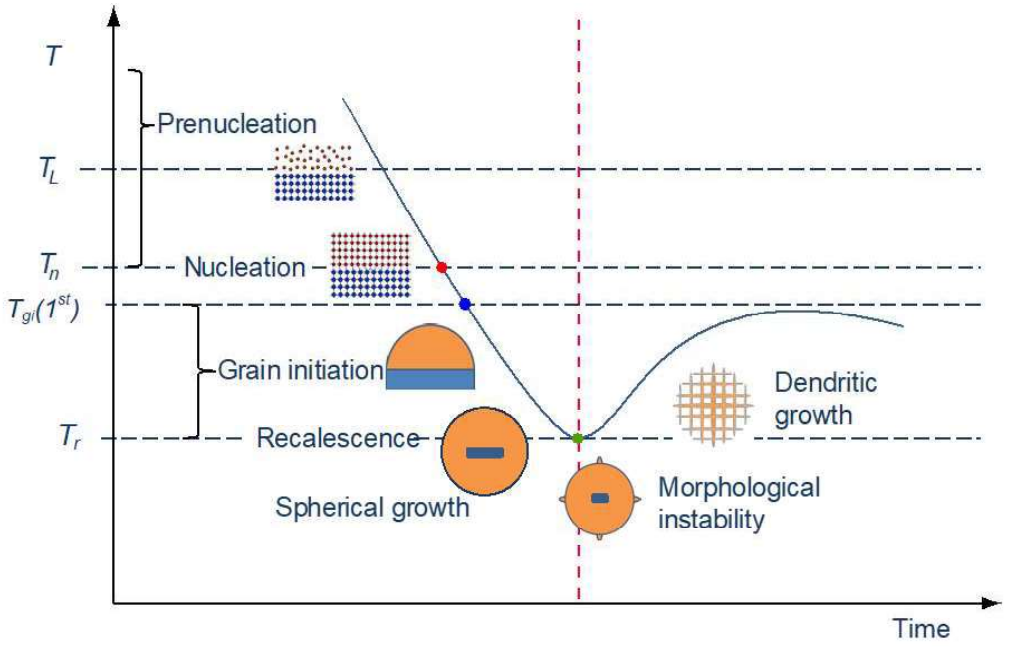

Fig. 2. A schematic cooling curve illustrating various stages of the solidification process by following a specific nucleant particle (in blue) that has initiated a grain in the solidified microstructure [58]. Early stages of solidification are delineated from other stags of solidification by the point of morphological instability (often close to the recalescence point under the TP-1 test condition), as marked by the vertical dashed red line. Please note that the length scale of the sketches increases with time during the solidification process.

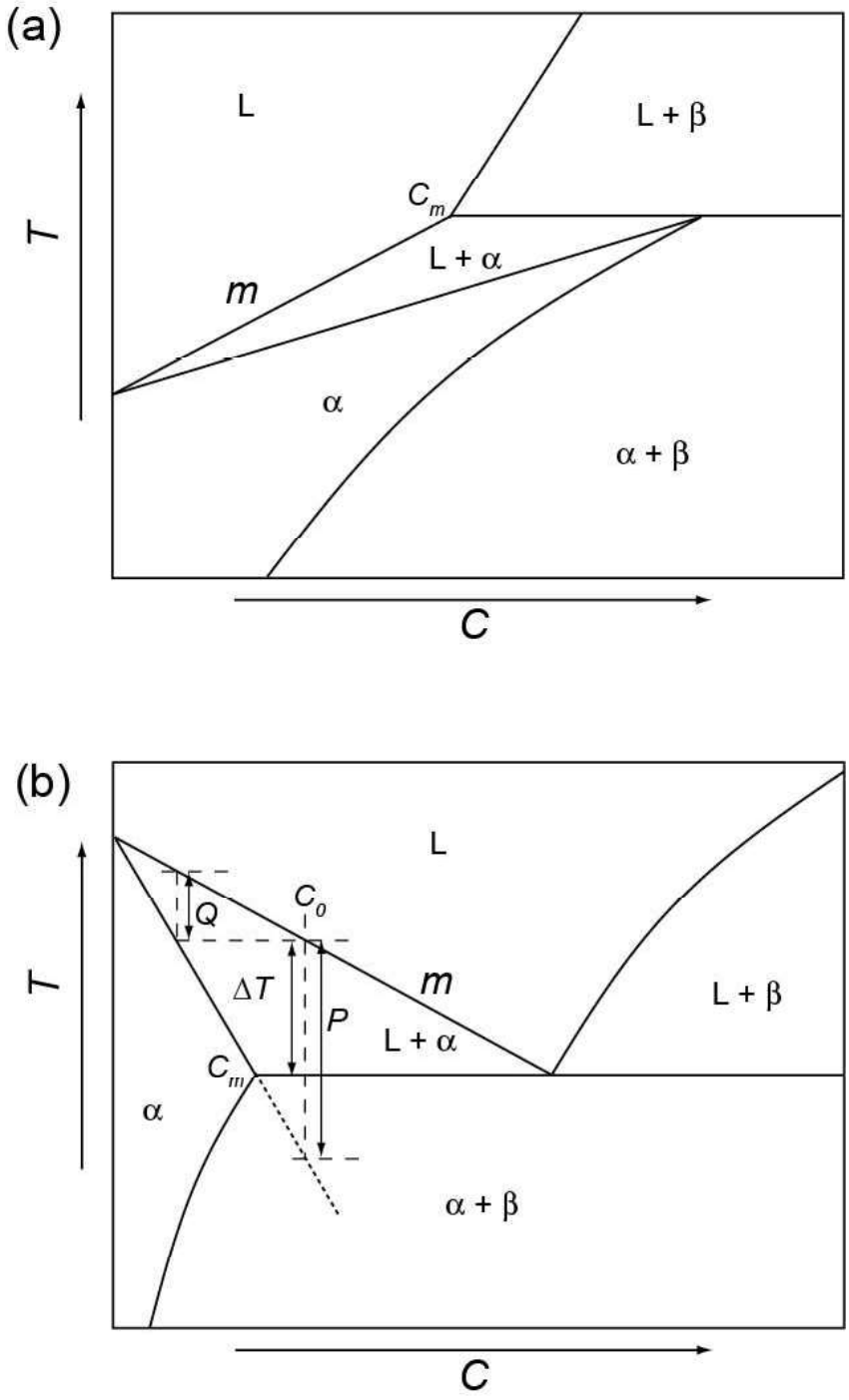

Fig. 3. Schematic binary phase diagrams of (a) peritectic and (b) eutectic systems showing parameters P, Q and ΔT. C_m in (a) and (b) is the peritectic point and the maximum solid solubility, respectively. For eutectic system (b), $\Delta T = P$ when $C_0 < C_m$, and $\Delta T < P$ when $C_0 > C_m$.

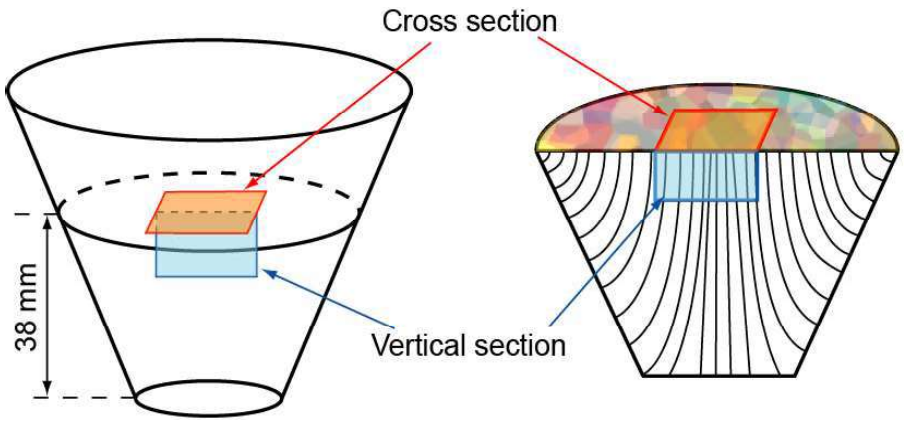

Fig. 4. Schematic illustration of a TP-1 casting sample showing that an equiaxed grain structure in a cross-section may not necessarily guarantee an equiaxed grain structure in the entire sample.

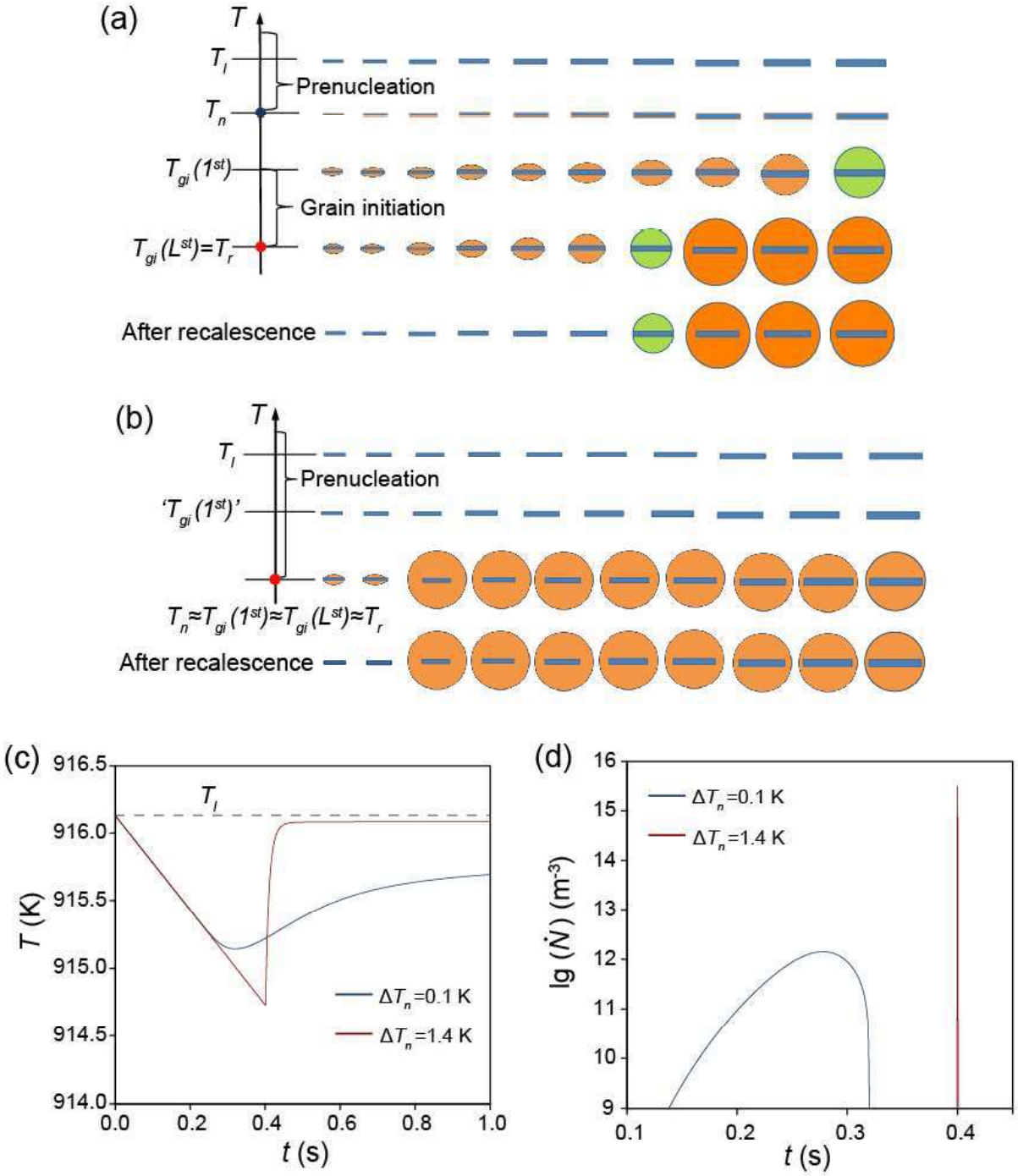

Fig.5. Schematic illustration of grain initiation behaviour during solidification of metallic alloys [58]. (a) Progressive grain initiation occurs when nucleation is easy and grain initiation is difficult; (b) explosive grain initiation occurs when nucleation is difficult and grain initiation is easy; (c) calculated cooling curves for typical progressive grain initiation (ΔT_n = 0.1K) and explosive grain initiation (ΔT_n = 1.4K); and (d) grain initiation rates for progressive grain initiation (ΔT_n = 0.1K) and explosive grain initiation (ΔT_n = 1.4K) corresponding to the cooling curves in (c).

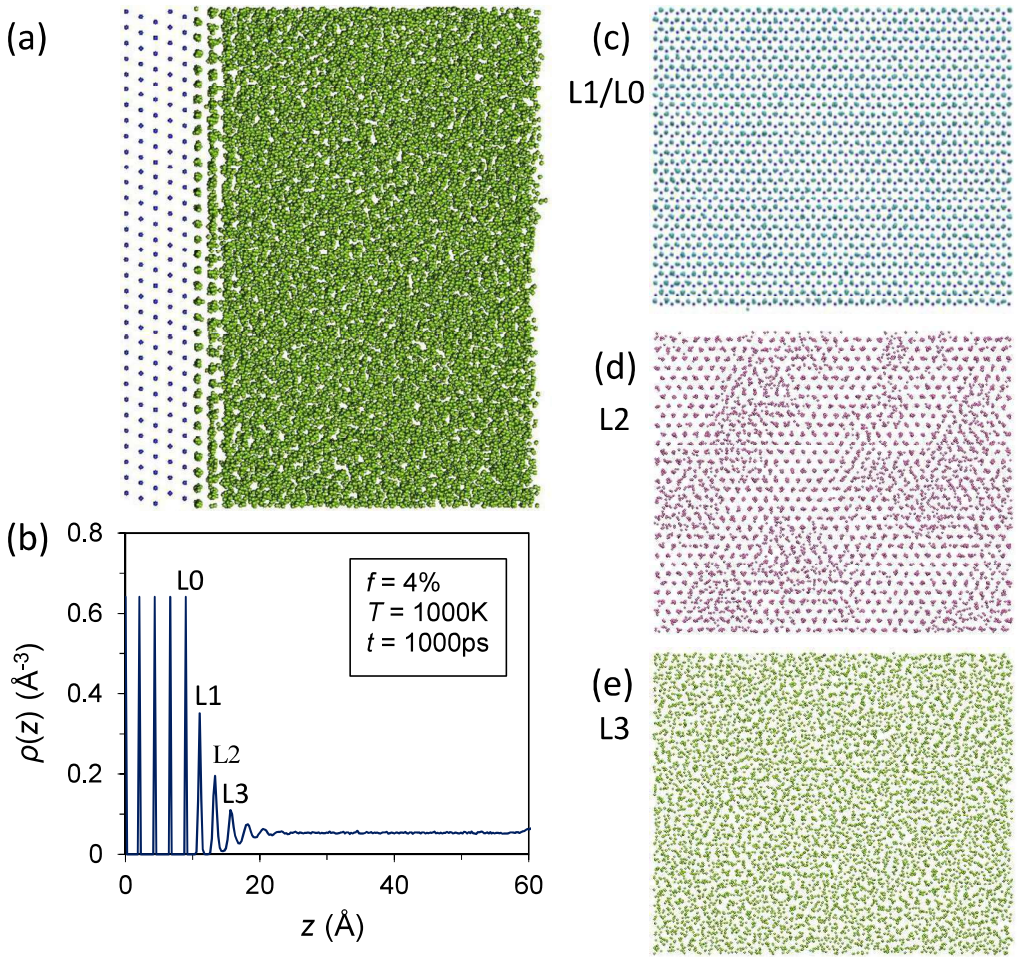

Fig.6. Prenucleation refers to the phenomenon of atomic ordering in the liquid adjacent to the liquid/substrate interface at temperatures above the liquidus [122]. (a) A snapshot (front view) of a generic system with 4% lattice misfit equilibrated at 1000K; (b) density profile corresponding to (a) showing atomic layering at the interface; (c) time-averaged atomic positions showing the atomic arrangement in the first layer (L1) on top of the substrate surface layer (L0); (d) atomic arrangement in the second layer (L2); and (e) atomic arrangement in the third layer (L3).

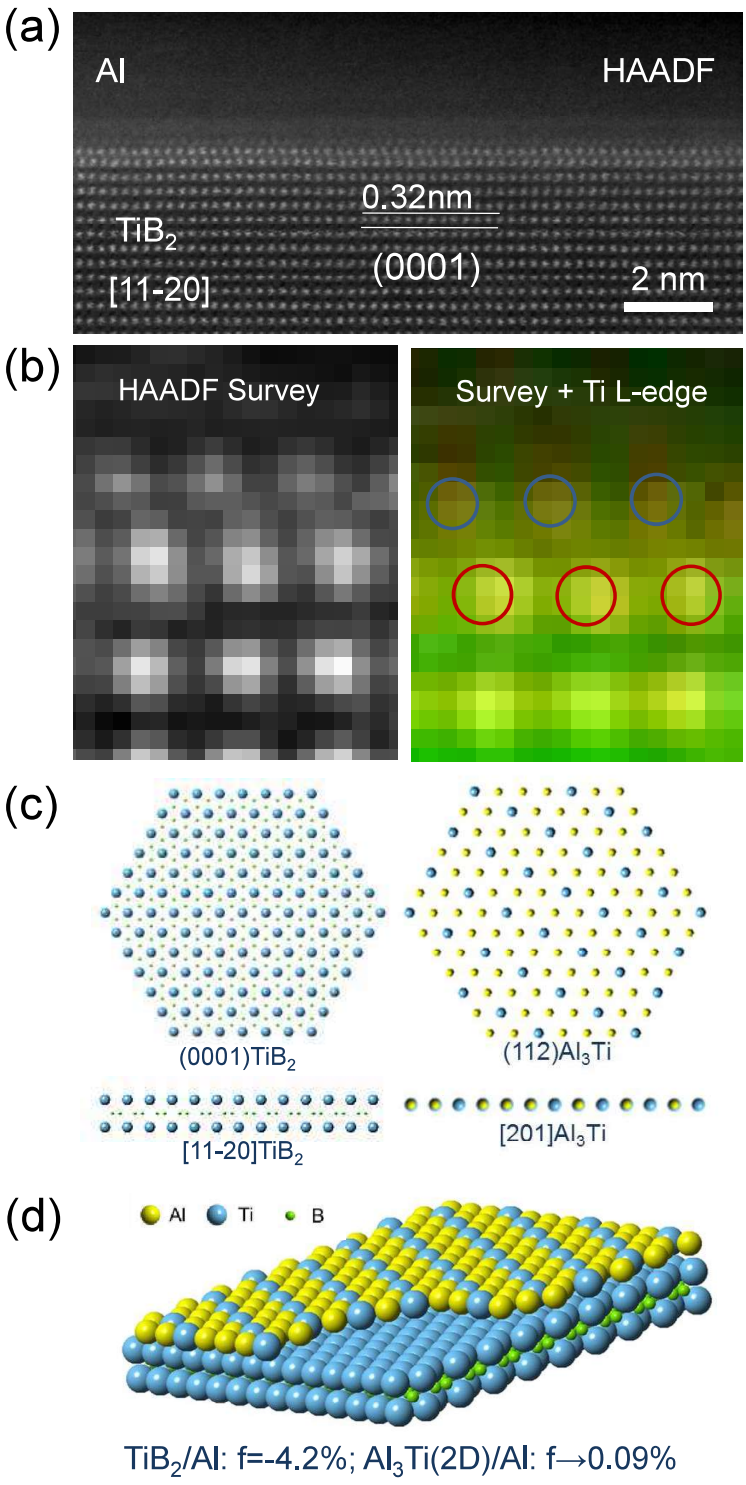

Fig. 7. Segregation of Ti at the Al/TiB_2 interface [3]. (a) High angle annular dark-field (HAADF) STEM image (Z-contrast) of α-Al /TiB_2 interface, showing the existence of an atomic monolayer on the (0 0 0 1) TiB_2 surface; (b) local Z-contrast HAADF and superimposition of the local Z-contrast image and Ti L-edge map across the α-Al/TiB2 interface. The atom columns with blue circles are Ti-rich columns, and those with red circles are Ti columns; (c) schematic illustrations of atomic arrangement in Ti-terminated (0 0 0 1) plane of TiB_2 surface and (1 1 2) plane of Al_3Ti; and (d) schematic illustration of 3D construction of the Al_3Ti 2DC on top of TiB_2.

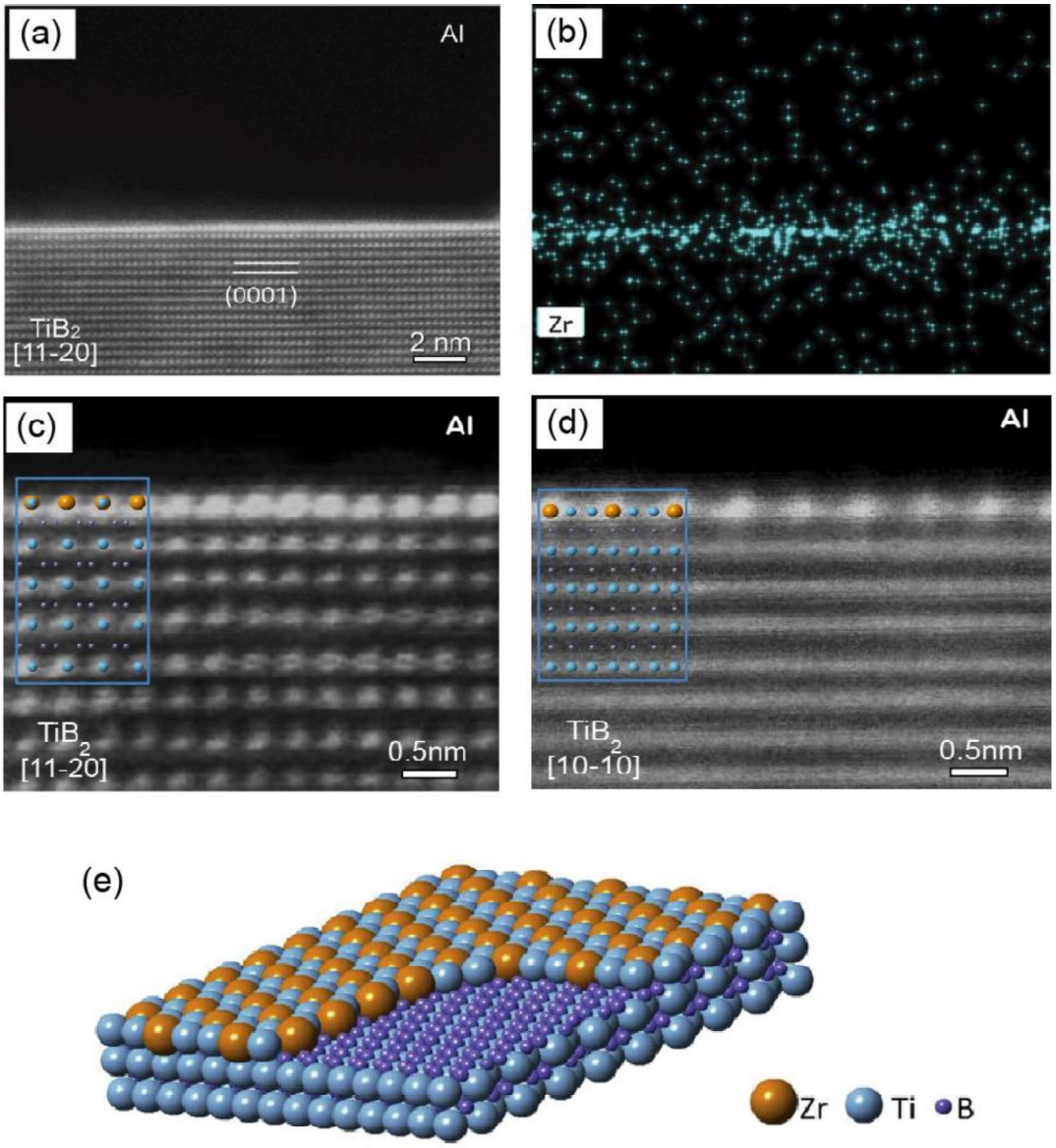

Fig. 8. Segregation of Zr at the Al/TiB_2 interface [4]. (a) High resolution STEM HAADF image across α-Al/TiB_2 interface viewed along [1 1 -2 0] TiB_2 direction; (b) Super-X EDS elemental mapping of Zr showing segregation of Zr on TiB_2 surface; high resolution STEM HAADF images of TiB_2 along (c) [1 1 -2 0], and (d) [1 0 -1 0] direction where the simulated results are shown as inserts in (c, d); (e) schematic illustration of 3D construction of the Ti_2Zr 2DC on top of TiB_2.

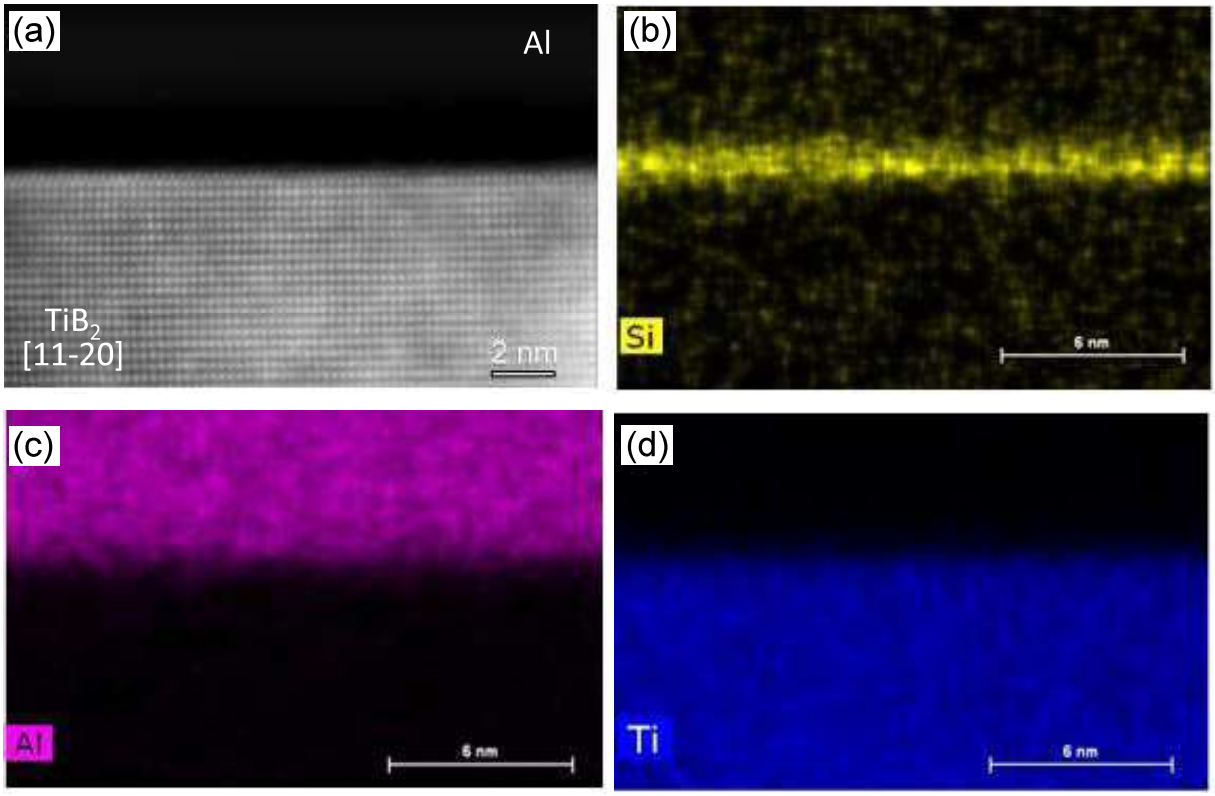

Fig. 9. Segregation of Si at the Al/TiB_2 interface in Al-Si alloys with high content of Si [10]. (a) High-resolution HAADF STEM image, and Super-X EDS elemental mapping of (b) Si, (c) Al, and (d) Ti, showing there is a Si-rich layer on the surface of TiB_2 particle.

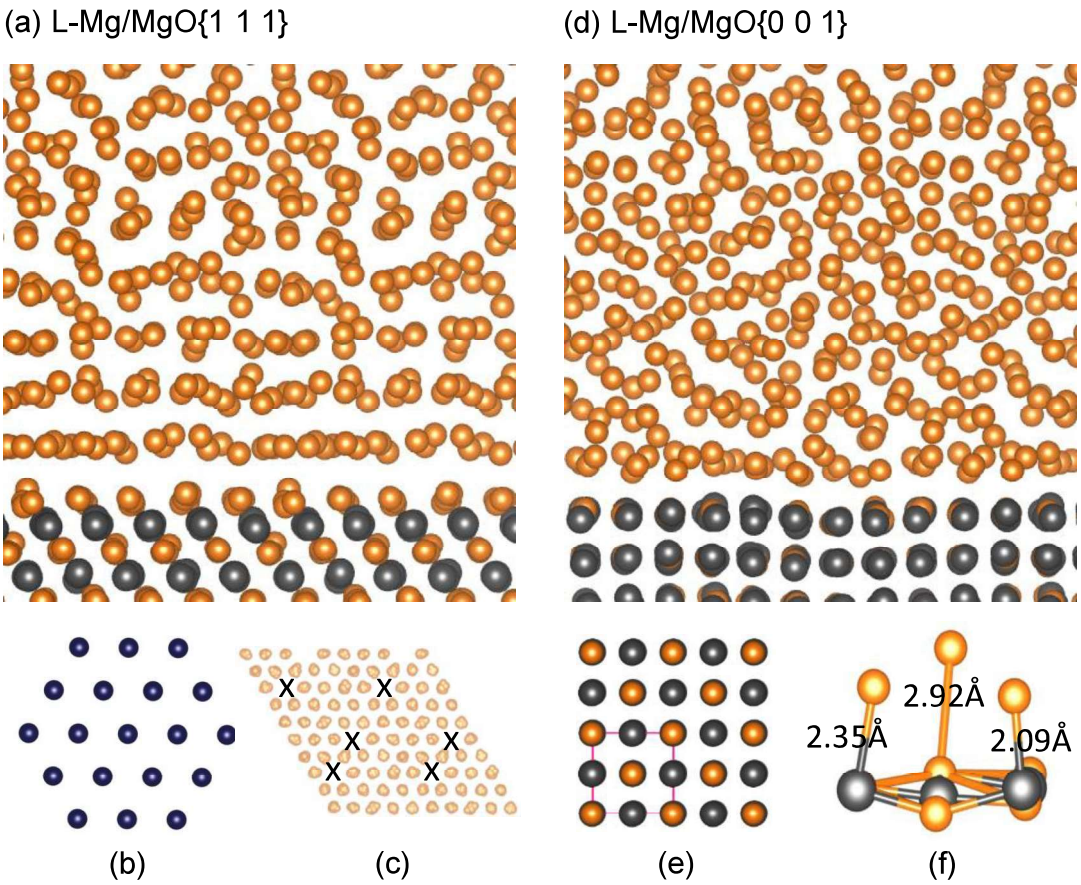

Fig. 10. The atomic arrangement at the interface between liquid Mg and MgO obtained by *ab initio* molecular dynamics (AIMD) simulations at 1000K [127]. (a) a snapshot of the L-Mg/Mg{1 1 1} system equilibrated at 1000K; (b) atomic arrangement at MgO{1 1 1} surface; (c) the terminating Mg layer in the L-Mg/MgO system contains vacancies (marked by "x") and thus becomes atomically rough; (d) a snapshot of the L-Mg/Mg{0 0 1} system equilibrated at 1000K; (e) atomic arrangement at MgO{0 0 1} surface (O is black and Mg is orange); (f) different bond lengths across the interface caused by chemical interaction between the liquid Mg and the substrate, suggesting Mg{0 0 1}is atomically rough.

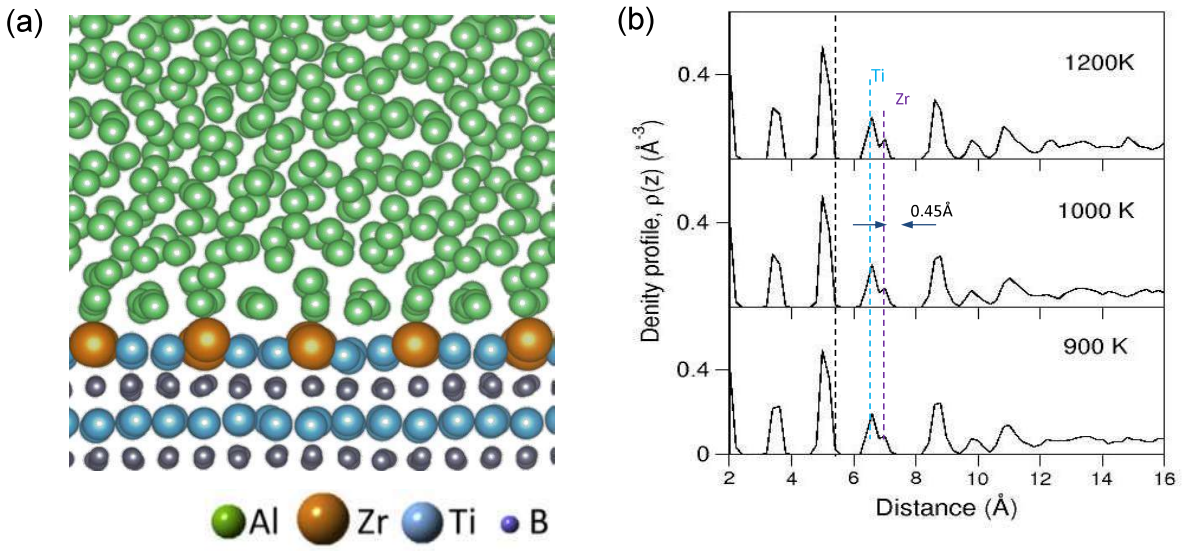

Fig. 11. (a) Snapshot of Al(liquid)/TiB_2 (Ti_2Zr 2DC) interface viewed along [1 0 -1 0] TiB_2 direction simulated at 1000 K, and (b) atomic density profiles $\rho(z)$ across the Al(liquid)/TiB_2 (Ti_2Zr 2DC) interface simulated at 900K, 1000K and 1200K, respectively. The dotted lines in (b) indicate the central positions of Ti and Zr atoms in the Ti_2Zr 2DC suggesting that Ti_2Zr 2DC is atomically rough [4].

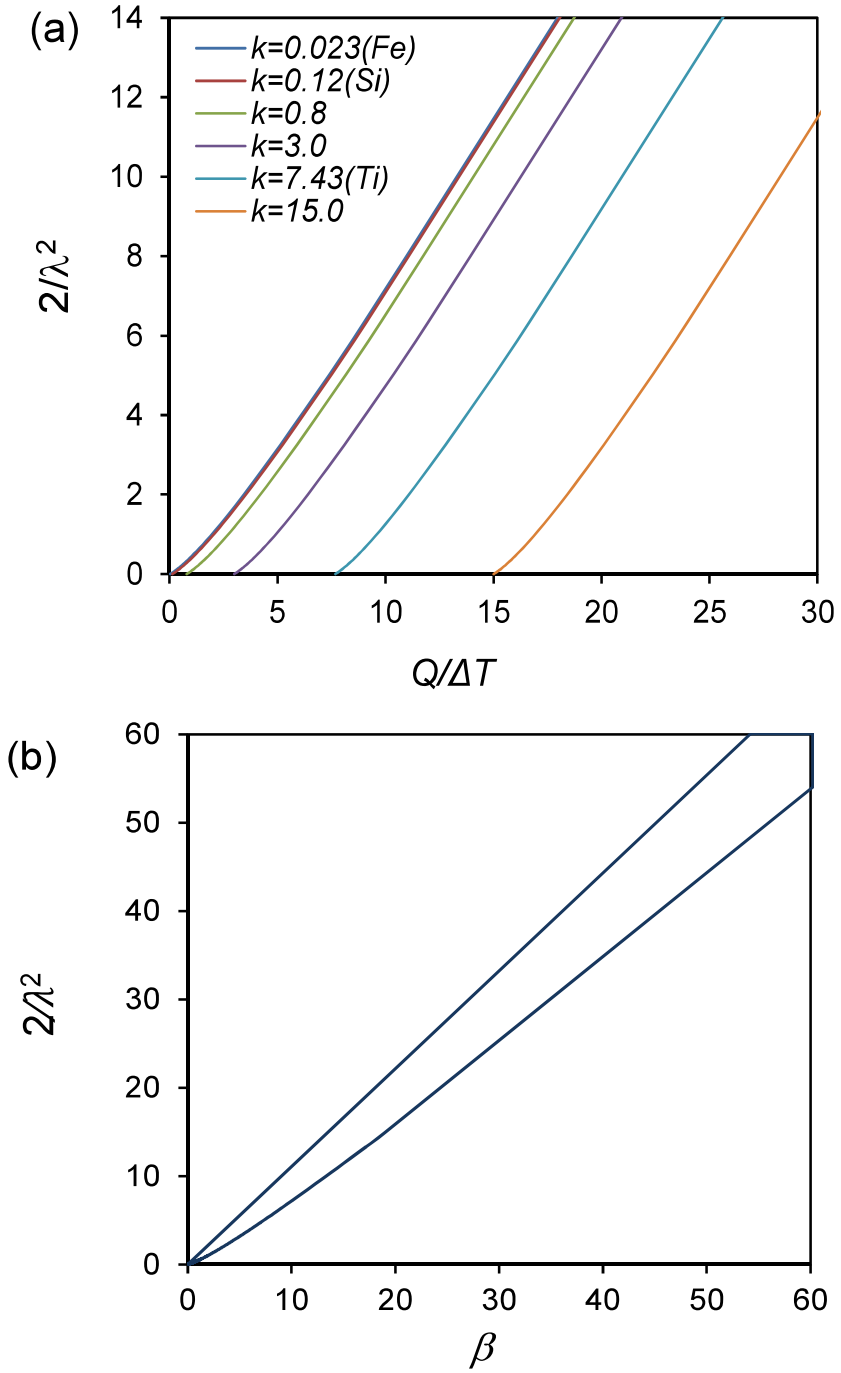

Fig. 12. Growth restriction coefficient ($2/\lambda^2$) for spherical growth during solidification of binary Al-alloys as a function of (a) $Q/\Delta T$; and (b) β showing that growth restriction coefficient is a unique function of β [89].

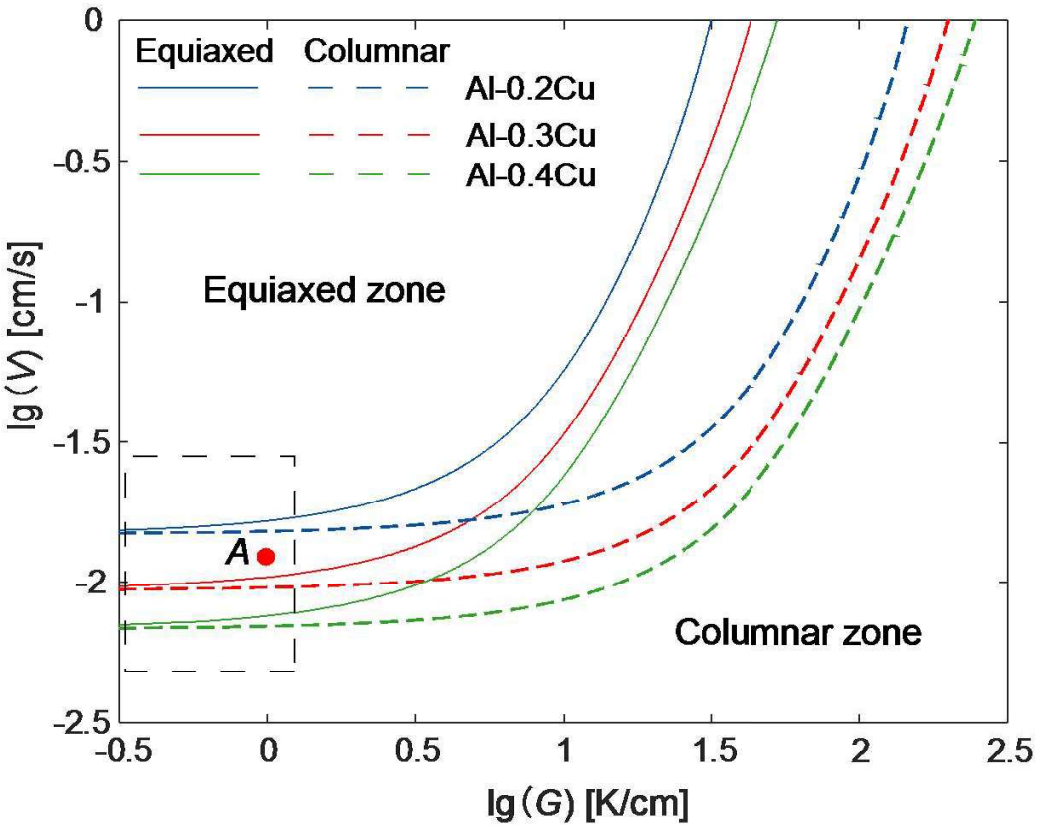

Fig. 13. The calculated CET map of Al-Cu alloys with the grain number density of 10^{11}m^{-3} and ΔT = 0.5K according to Hunt's CET model [81]. When the temperature gradient is small (around 1K/cm) solidification becomes quasi-isothermal, and the transitional zone becomes very narrow. Consequently, the grain structure is identified as either equiaxed or columnar. Under the quasi-isothermal condition, $\beta = 1.14$ can be used as a criterion for CET.

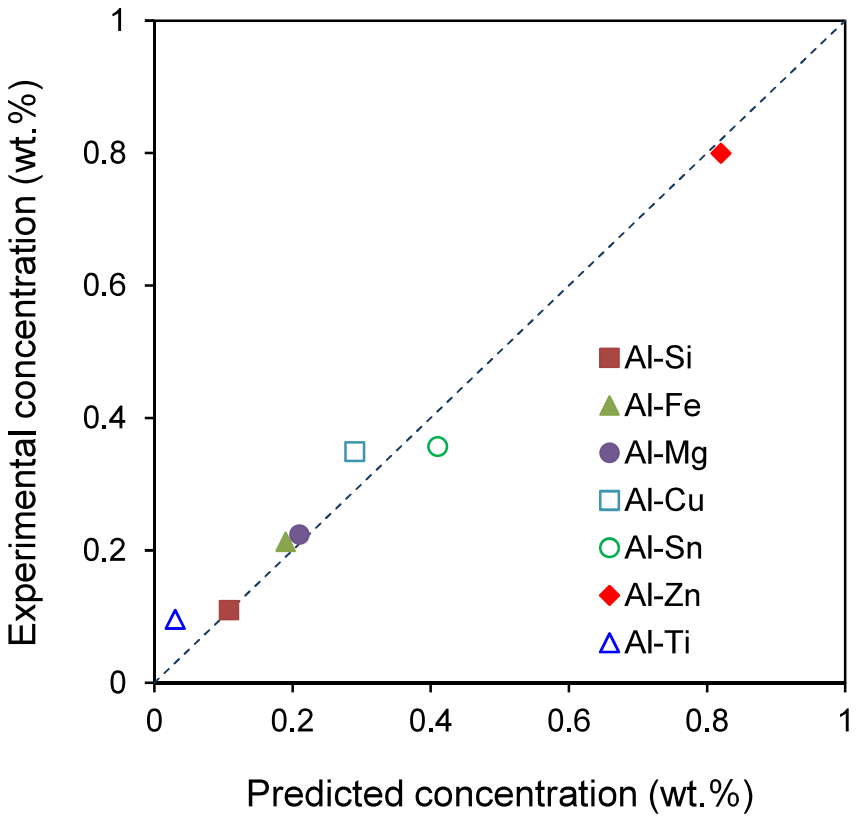

Fig. 14. Comparison between the predicted composition for CET by β = 1.14 and the experimental results for binary Al-alloys [89].

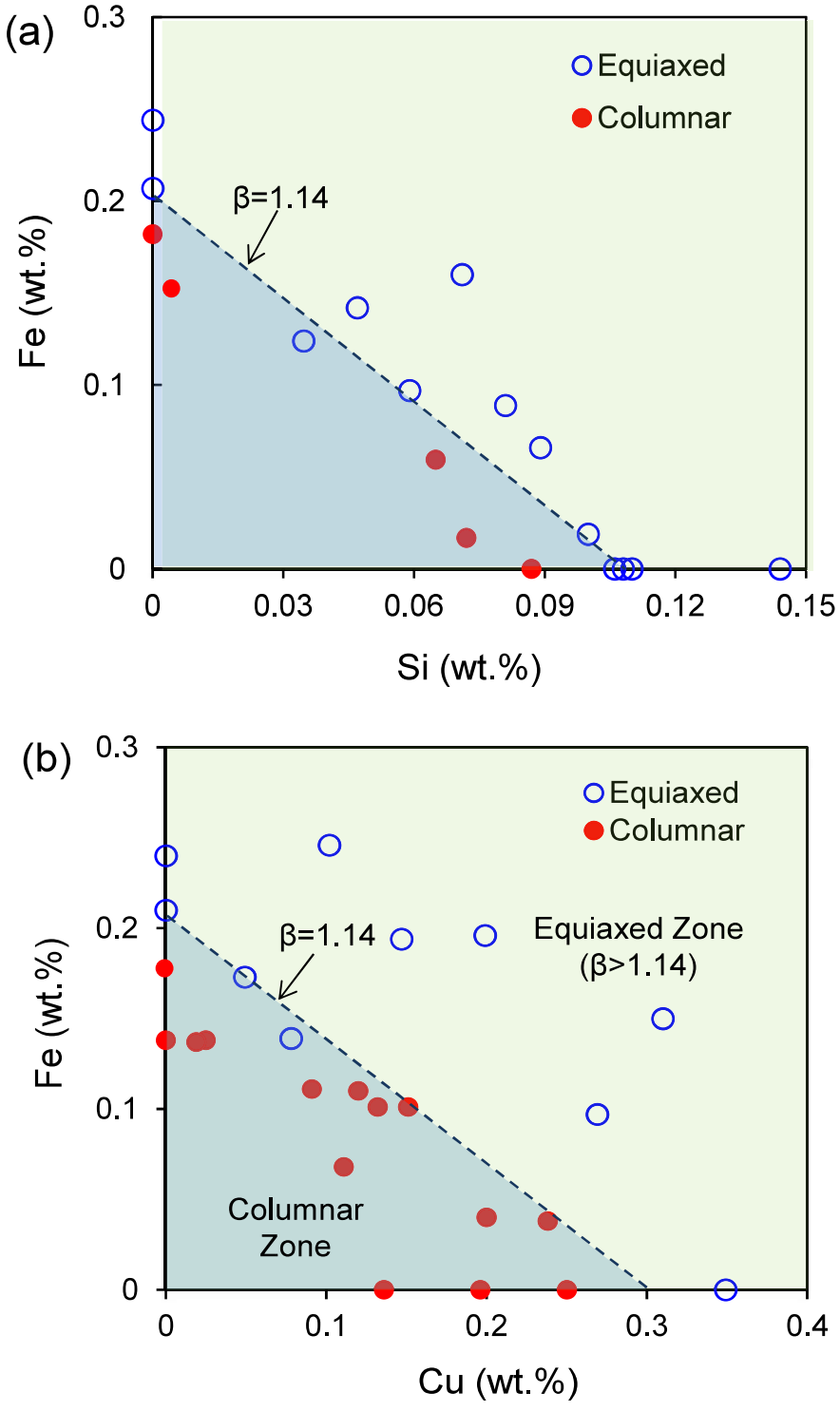

Fig. 15. Microstructural map predicted by β = 1.14 for the ternary Al-alloy systems in comparison with the experimental results. (a) Al-Fe-Si; and (b) Al-Fe-Cu.

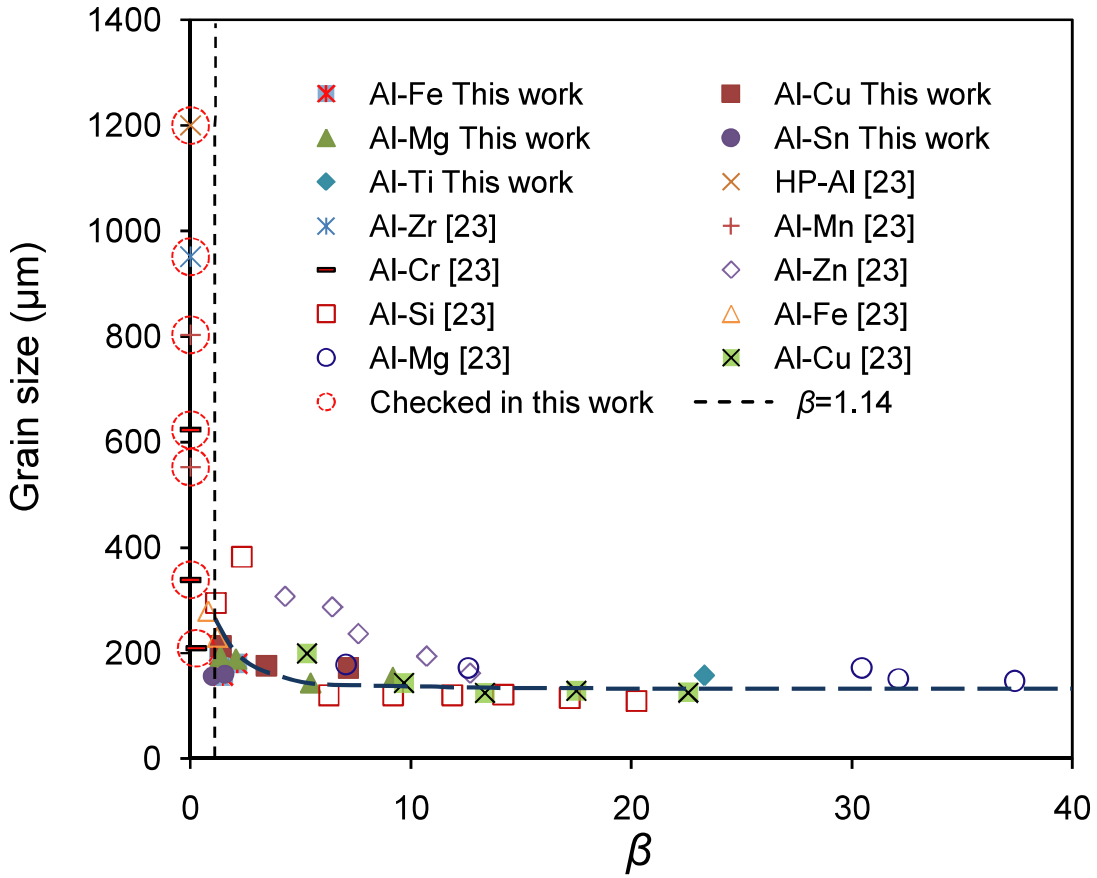

Fig. 16. Grain size data of binary Al-alloys from both this work and Spittle and Sadli [23] as a function of β calculated with $\Delta T = 0.5$K. The open dashed circles mark these alloys from Spittle and Sadli [23] that were assumed to have an equiaxed grain structure but confirmed to have a fully columnar grain structure after repeating Spittle and Sadli's experiments. The long-dashed line shows the trend of grain size; and the short-dashed line represents $\beta = 1.14$. All alloys with $\beta < 1.14$ have a columnar structure.

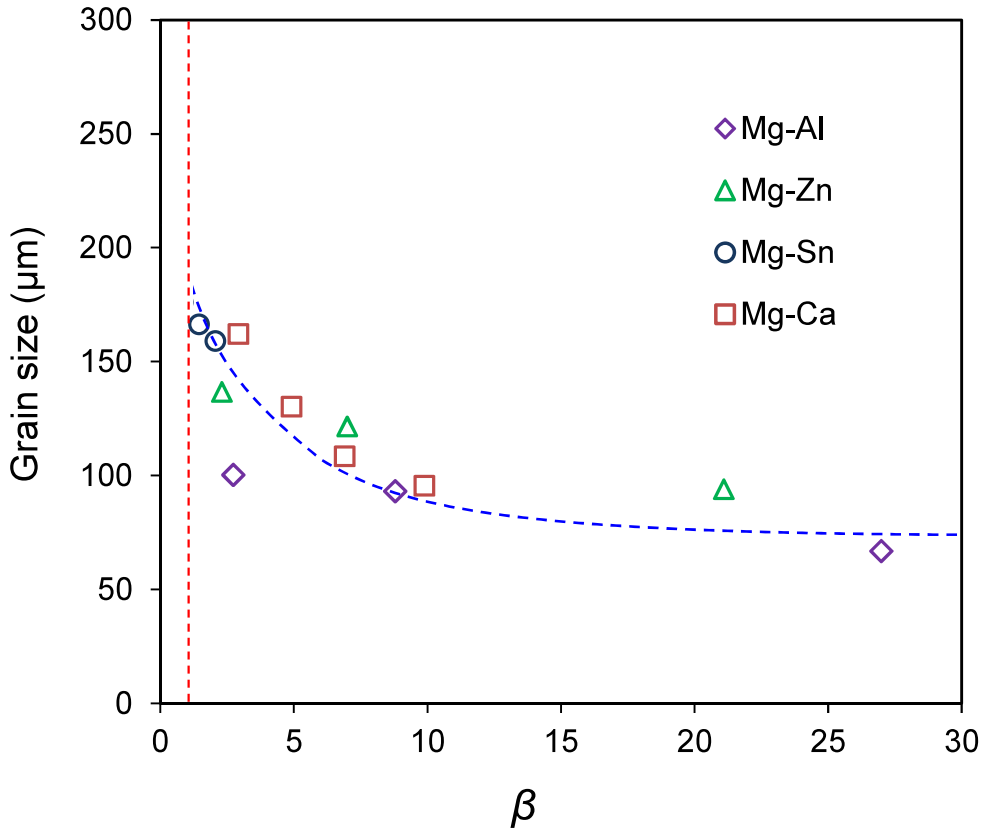

Fig. 17. Grain sizes of binary Mg-alloys (Mg-Al, Mg-Ca, Mg-Sn and Mg-Zn) as a function of β, showing the effects of solute content on grain size. The dashed blue line is the trend for grain size and the dashed red line represents $\beta = 1.14$. The undercooling used for the calculation of β is 1.2K.

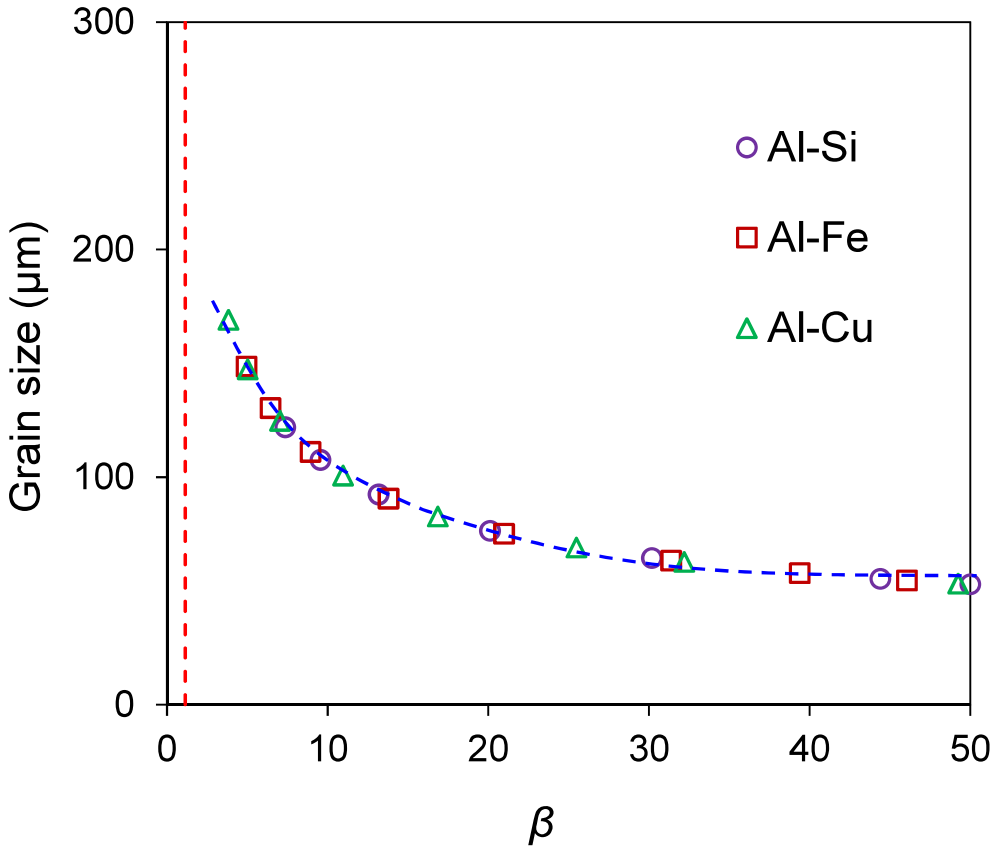

Fig. 18. The numerically calculated grain size as a function of β calculated using the maximum undercooling at recalescence. The blue dashed line is the fitted trend for grain size, and the red dashed line represents β=1.14.

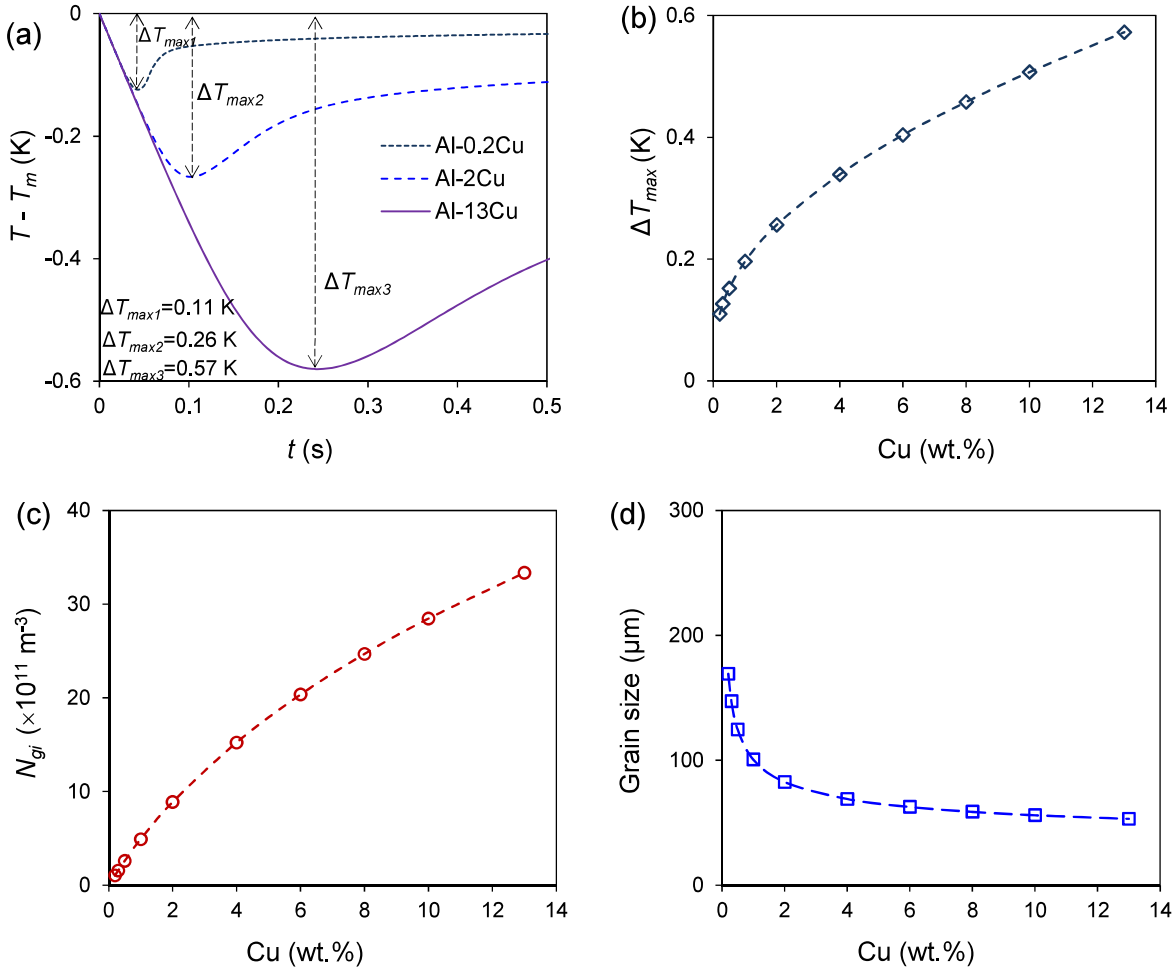

Fig. 19. (a) The calculated cooling curves of Al-0.2Cu, Al-2Cu and Al-13Cu alloys, showing that recalescence is delayed to a lower temperature by increasing the solute contents; and (b) the calculated ΔT_{max}, (c) the total number density of initiated grains (N_{gi}) and (d) grain size for Al-Cu alloys.

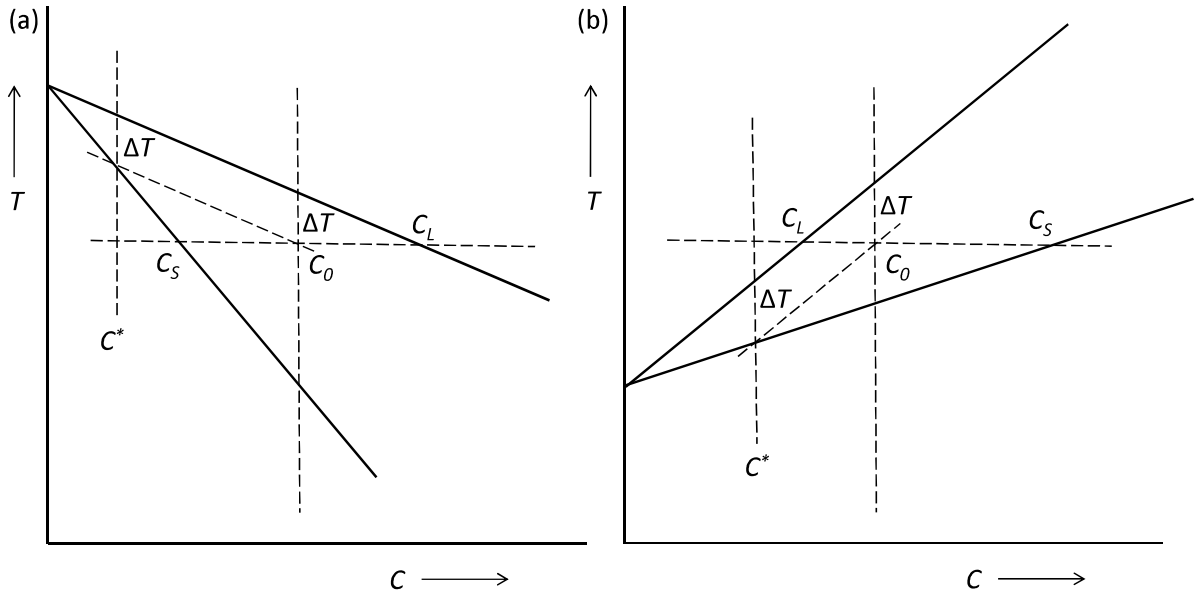

Fig. 20. Schematic illustration of the concept of critical solute concentration C^* for binary alloy systems [89]: (a) the eutectic system; and (b) the peritectic system. In both cases, when $C_0 < C^*$, solidification becomes partitionless and therefore there is no growth restriction ($\beta = 0$); whereas when $C_0 > C^*$, growth restriction increases with increasing C_0 as described by Eq. (12).

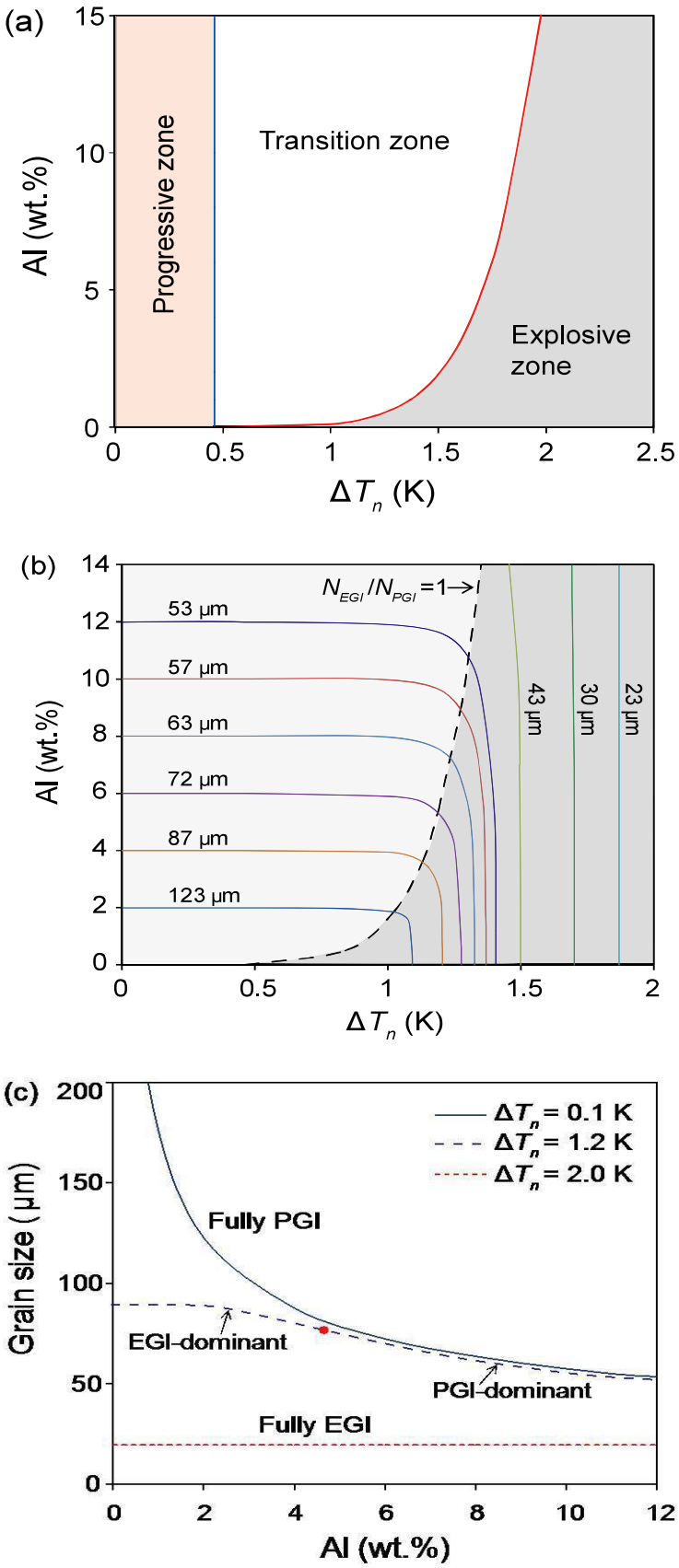

Fig. 21. Solute effect on grain initiation and grain size of Mg-Al alloys [58]. (a) Calculated grain initiation map showing three zones: progressive zone, explosive zone and transition zone; (b) calculated grain refinement map, where the solid lines are the iso-grain-size lines, and the dashed line represents $N_{EGI} = N_{PGI}$ delineates between the EGI dominant and PGI dominant zones. (c) The solute

effect on grain size for different grain initiation behaviours. The parameters used for the calculations can be found in Ref. [58].

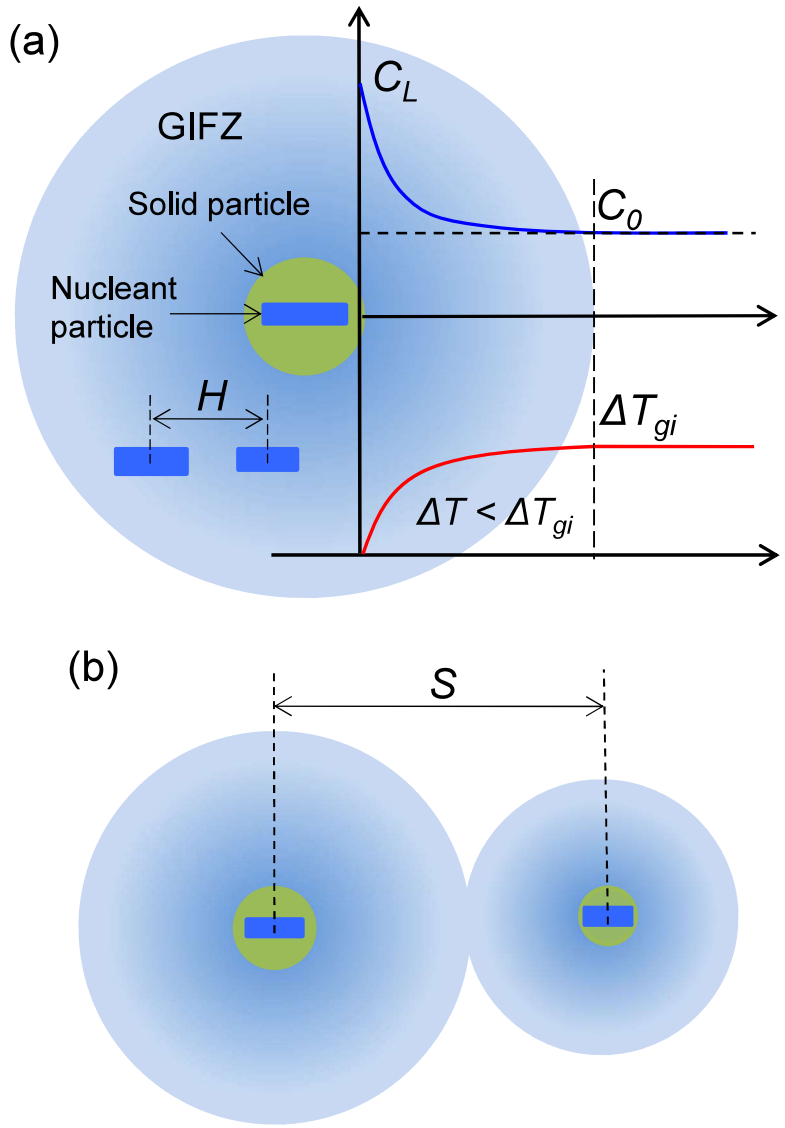

Fig. 22. (a) The schematic illustration of (a) the grain initiation free zone (GIFZ) and (b) the overlap of solute fields of two growing solid particles [157]. *H* is the distance between the two nearest nucleant particles, and *S* is the distance between the two nearest solid particles.

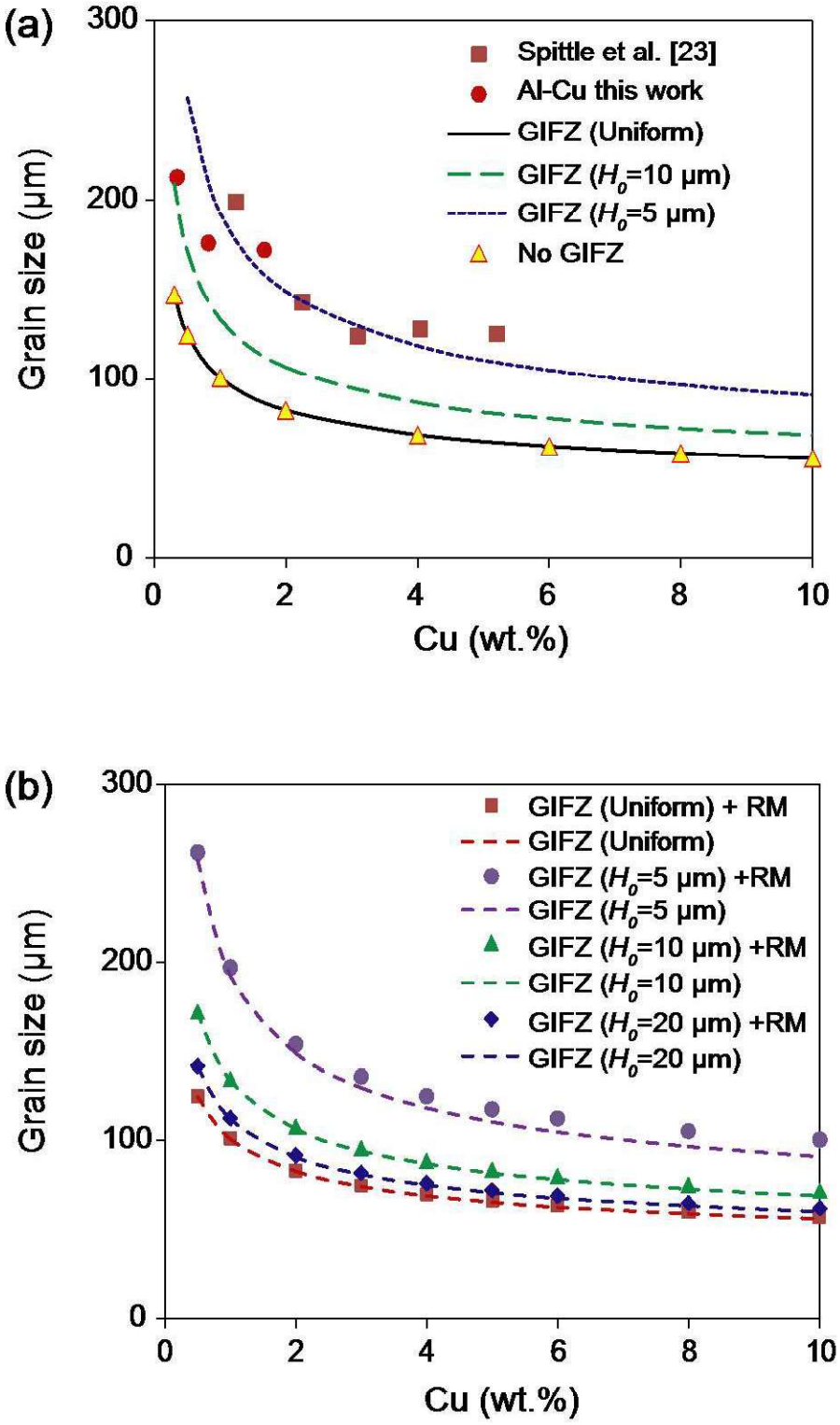

Fig. 23. (a) The calculated grain size of Al-Cu alloys with and without GIFZ in comparison with the experimental data [157]. With considering the GIFZ the agglomeration effect is assessed by varying H_0. (b) The calculated grain size with and without considering solid particle re-melting (RM), showing that the influence of solid particle re-melting on grain size is very limited and can be therefore ignored.